Pontificia Universidad Católica del Perú

Escuela de Posgrado

Tesis

Design of a self-adjusting antenna feed for a homologous designed tiltable 20m-radio-telescope

Para obtener el grado de Magíster
en Ingeniería Mecatrónica

Presentado por: Martin Böhme

Professor Responsable (TU Ilmenau): AOR PD Dr.-Ing. Tom Ströhla

Professor Responsable (PUCP): Prof. Dr. Jorge Arturo Heraud Pérez

Fecha y Lugar: 17/11/2015, Lima

TECHNISCHE UNIVERSITÄT
ILMENAU

PONTIFICIA
UNIVERSIDAD
CATÓLICA
DEL PERÚ

Fakultät für Maschinenbau

Instituto de Radioastronomía

Assignment Master Thesis

for Martin Böhme, B.Sc.

Topic: Design of a self-adjusting antenna feed for a homologous designed tiltable 20m-radio-telescope

Radio telescopes are exposed to gravity, wind and temperature. Especially tiltable telescopes are influenced by these forces. The institute for radioastronomy INRAS of the Pontificia Universidad Católica del Perú is designing a new 20m-radio-telescope. The object of this thesis is to determine the deformation of the telescope structure through gravity, wind and temperature. Then an actuation principle will be designed to adjust the antenna into the new focal point. The purpose is to optimize the antenna efficiency which otherwise decreases with deformation.

The following points are part of the thesis:

- research on the state of the art of homologous designed radio telescopes
- implementing mechanical structure model in a FEM-Software (i.e. ANSYS)
- determine the deformations of the reflector surface caused by gravity, wind and temperature gradient
- creating an algorithm to determine paraboloidal parameters of the surface
- estimate requirements on an actuator for the adjustment of the antenna
- mechatronical design of an actuator to adjust the antenna

This thesis serves to receive the master double degree of the Technische Universität Ilmenau (TU Ilmenau) and the Pontificia Universidad Católica del Perú (PUCP) in Mechatronical Engineering.

Date of issue	20.04.2015
Professor of the PUCP Lima	Prof. Dr. Jorge A. Heraud P.
Professor of the TU Ilmenau	Priv.-Doz. Dr.-Ing. habil. Tom Ströhla

Lima, 07 April 2015
Place, date

Jorge Heraud
Prof. Dr. Jorge A. Heraud P.

Ilmenau, den 15.4.2015
Place, date

Priv.-Doz. Dr.-Ing. habil. Tom Ströhla

Lima, 07. April 2015
Place, date

Martin Böhme, B.Sc.

Declaration of academic integrity / Eigenständigkeitserklärung

Hiermit versichere ich, dass ich die vorliegende Arbeit selbstständig verfasst und keine anderen als die angegebenen Quellen und Hilfsmittel benutzt habe, dass alle Stellen der Arbeit, die wörtlich oder sinngemäß aus anderen Quellen übernommen wurden, als solche kenntlich gemacht sind und dass die Arbeit in gleicher oder ähnlicher Form noch keiner Prüfungsbehörde vorgelegt wurde.

Hereby I declare that I wrote the present work independently and that did not use any literature source or aids other than quoted.

Martin Böhme
Ilmenau, den 17. November 2015

Kurzfassung

Radioteleskope sind verschiedenartigen Umwelteinflüssen ausgesetzt. Dadurch hervorgerufene Verformungen der Reflektoroberfläche verändern deren geometrischen Eigenschaften und können die ursprüngliche Position und Form des Brennpunkts verändern. Eine Abweichung dieses Brennpunkt von der Lage der Primärantenne beeinflusst die Leistungsfähigkeit des Teleskops. Die vorliegende Arbeit zeigt eine Methode zur theoretischen Abschätzung der Verformung durch das Eigengewicht des Reflektors des INRAS RT–20. Jene nach der Idee des homologen Designs von Hoernerѕ konstruierten Teleskopen weisen eine Stützstruktur auf, die die Reflektorfläche unabhängig vom Elevationswinkel in einer der ursprünglichen Form ähnlichen Gestalt halten. Somit kann die Verformung durch das Nachführen der Primärantenne ausgeglichen werden. Grundlage der Untersuchung ist ein vorhandenes Strukturmodell des RT–20–Teleskops. Zusammen mit den zugehörigen Geometriedaten und Materialparameten wird ein Finite-Element-Modell erstellt. Für dieses wird ein Belastungsfall mit dem Eigengewicht für verschiedene Elevationswinkel simuliert. Um die deformierte Reflektorfläche mathematisch zu beschreiben und den passenden Brennpunkt zu bestimmen wird eine parametrisierte Form eines Best-Fit-Paraboloids erörtert. Für die Ermittlung der Parameter werden drei Optimierungsalgorithmen in Matlab ausgeführt und miteinander verglichen. Daraus wird die Verschiebung des Brennpunkts (Defokussierung) ermittelt und der Bedarf einer Korrekturbewegung für die Primärantenne abgeschätzt. In einem Entwurfsprozess werden nach den Ideen der VDI2221–Norm technische Prinzipe für ein Aktuierungssystem entwickelt und bezüglich ausgewählter Kriterien gegeneinander abgewogen. Als Resultat dieses Bewertungsprozesses wird eines der Prinzipe erwählt und spezifiziert. Für die spätere Umsetzung werden Komponenten vorgeschlagen, Bauteile vorbereitend konstruiert und in einer CAD–Software zu einer funktionierenden Baugruppe zusammengefügt.

Abstract

Radio telescopes are exposed to various environmental conditions. These can produce deformations of the reflector surface that will have impact on its paraboloidal characteristics determining the position and shape of the focal point. A misalignment between the reflector focal point and the radiation–receiving primary antenna influences the performance of the telescope. The actual work presents a method to estimate theoretically the dead–weight induced deformation of the reflector surface for the INRAS PUCP RT–20 radio telescope. Such homologous designed telescopes consist of a backing structure supporting the reflector surface to retain a shape familiar to the original one and independent of the elevation angle. So it is possible to compensate the deformation by the adjustment of the primary antenna. The analysis of the deformation is done for an existing structural model of the RT–20. This model is meshed with the corresponding geometrical and material properties. In a finite–element software the load situation due to the telescope's dead weight is simulated for different elevation angles. To describe the deformed reflector surface in a mathematical way an expression for a parametrized best-fitting paraboloid is derived. To determine the fit-parameters for the discrete point set, three optimization algorithms are executed in MATLAB and their results compared. Based on this, the need of a re-alignment of the primary antenna is demonstrated. Thereupon a design process for an actuation system intended for the corrective movement is performed, following the ideas of the VDI2221–norm. Several mechanical concepts are presented and evaluated in relation to their suitability for the main needs. Based on this assessment, a parallel–kinematic mechanism is chosen as the most convenient concept. This is examined in more detail, including a deviation for the inverse kinematics. For this concept, a preliminary selection of specific components is done and assembled in a CAD–prototype.

Contents

Nomenclature

Symbol / Abbr.	Description	Unit
$\boldsymbol{d}_i$	displacement vector of surface node i	m
$\boldsymbol{g}$	gravity vector	m/s^2
$\boldsymbol{K}$	stiffness matrix	N/m
$\boldsymbol{v}_i$	position vector of a surface node i	m
δ	displacement in y-direction (axial)	m
ϵ	surface error	m
λ	wavelength	m
λ_{gr}	minimum wavelength set by the gravitational limit	m
λ_{th}	minimum wavelength set by the thermal limit	m
ϕ_{x}	angle around x-axis	°
ϕ_{z}	angle around z-axis	°
ψ	elevation angle	°
A_{f}	projected area normal to the wind	1
B, b	width of a framework bar	m
C_{f}	net force coefficient	1
D	diameter	m
D_{f}	change of the focal distance	m
F	force	N
f	frequency	Hz
h	coefficient for the focal shift	1
L, l	height of a framework bar	m
q_{y}	dynamical pressure at height y	1
T	temperature	K
u	vertex shift in x-direction	m
$u_{\mathrm{F,rot}}$	focus shift in x-direction due to rotation around ϕ_z	m

u_{F}	focus shift in x-direction	m
u_{P}	shift of the primary antenna in x-direction	m
v	vertex shift in y-direction	m
$v_{\mathrm{F,rot}}$	focus shift in y-direction due to rotation around ϕ_z	m
v_{F}	focus shift in y-direction	m
v_{P}	shift of the primary antenna in y-direction	m
W	weight	N
w	vertex shift in z-direction	m
W_{B}	elastic section modulus	mm^3
W_G	gust effect factor	1
x_{off}	offset in x-direction between antenna and focus	m
y_{off}	offset in y-direction between antenna and focus	m
Abbr.	Abbreviation	
ANSYS	Software for FEM-Simulations from *Ansys Inc.*	
CAD	computer–aided design	
CCD	Charge-coupled Device	
CFD	Computational-Fluid-Dynamic	
DC	Direct current	
DOF	degree of freedom	
FEM	Finite-Element Method	
INACOM	lnvestigación Asistida por Computadora	
INRAS	Instituto de Radioastronomía PUCP	
LES	Large-Eddy Simulation	
PUCP	Pontificia Universidad Católica del Perú	
RANS	Reynolds Averaged Navier-Stokes	
RMS	root-mean-square	
RMSE	root-mean-square error	
RT	Radio telescope	
SETI	Search for Extraterrestrial Intelligence	
VDI	Verein Deutscher Ingenieure	
VIRAC	Ventspils International Radio Astronomy Center	
VLBI	Very Long Baseline Interferometry	

CHAPTER 1

Introduction

For thousands of years humans are studying celestial objects. Over the time optical observations increased the knowledge about them and these remote processes. Then the invention of optical telescopes enhanced the possibilities for the studies immensely. More than one hundred years ago, the theory predicted electromagnetic radiation with frequencies of X-rays and radio waves, emitted by celestial objects. Jansky discovered the first extraterrestrial radio source in the year 1933. The first radio telescope for exclusively astronomical use was constructed by Reber in the year 1937. Such a radio telescope uses an antenna and a corresponding receiver to collect and detect celestial radio signals. The antenna can be assumed as the pendant to the lens or mirror of an optical telescope. The whole setting of an antenna, the receiver and following processing units can be referred as *radio telescope*. The radio astronomy became an important part of the astronomy because of the long waves. In contrast to optical telescopes, observing the electromechanical spectrum of light, a radio telescope is working with much lower frequencies. The study of celestial objects emitting radiation requires the observation of the radio spectrum with a range from 10 MHz up to 30 GHz, covering most of the radio sources. Studying the sky at this wavelengths delivers an entire new perspective, contrary to the experiences from the optical impression. Some objects are may not visible in the spectrum of light but radiating at radio wavelength. In addition some objects opaque to light are frequently transparent for radio waves.[CH69][Kra93]

But the major wavelength reduces the amount of detail to see in comparison to optical telescopes. A radio telescope has to be millions of times bigger, to get the same resolution. This yields to huge mechanical structures. Since a radio telescope is a mechatronic structure, its performance depends on both the mechanical and electrical properties influencing each other. Radio telescopes may be exposed to harsh environment conditions like the influences of gravity, wind loads and high temperature gradients. The antennas need a high precision of the reflector surface. Any departure

of the reflector from the intended geometrical shape causes fuzziness of the focal point and reduces the antenna performance significantly. In addition the space and time coherence of the received wave is disturbed. [WDQ+04]

Over the time there was an increasing need for very large reflectors and a higher surface accuracy at once. Until the 1960s the telescopes were constructed to provide a sufficient stiffness against the gravity and wind loads. Scaling up the diameter runs into structural or rather mechanical limitations, since . In the year 1967 VON HOERNER presented his idea of the homologous design. Such a design allows the reflector backing structure to deform significantly. But due to its construction it transforms from the original shape into a familiar one. So a paraboloid of revolution retains in a paraboloidal shape, but possibly changing the focal distance as well as the position and orientation in space. So if it is possible to predict the deformations by measurements or simulations, a mathematical description of the reflector surface and the position of the focus can be found. Since the location of the new focal point is known, an adjustment of the primary antenna can refocus the telescope to minimize the gain loss of the telescope.[Hoe67a][Baa07]

The *Institute for Radio Astronomy INRAS*, located in Lima, was founded in the year 2009. The first main project was the construction of a world class radio telescope with an aperture-diameter of 20 m called RT-20. The fully steerable telescope is intended to cover a frequency range from 327 MHz up to 15 GHz. Located in Peru, in the southern hemisphere and with a long distance to other radio telescopes it will offer a significant contribution to Very Long Baseline Interferometry (VLBI), studies of active and normal galaxies, mapping and observation of radio sources, satellite tracking and other investigations. In addition it is intended to provide international collaboration with other projects like SETI (Seach for Extraterrestrial Intelligence). [HFA+14][FHY+13]

To be a high–precision instrument the radio telescope RT–20 has to provide an exceeding surface accuracy and the best possible antenna performance. To offer a well-focussed telescope with a minimum gain loss, it was constructed following the ideas and methods of the homologous design. This work analyses the often specific approaches for the construction of several radio telescopes and transfers this knowledge to the RT–20. It covers the simulative prediction and estimation of the expected reflector deformations. Based on this it will implement a mathematical description of the reflector geometry and a method to determine a possible shift of the focal point. Pursued by the idea of the simple compensation of the focal shift, an actuation system for the primary antenna will be discussed and worked out.

CHAPTER 2

State of the art for the focal point correction of homologous designed radio telescopes

2.1 Mechanical design of steerable radio telescopes

2.1.1 General construction

Figure 2.1 shows the radio telescope of the Max Planck institute for radio astronomy in Effelsberg. Its development started in the 1960's and is a typical representative of modern telescopes following the homologous design method by Hoerner [Hoe67a].

The mechanical system of a radio telescope basically consists of an antenna feed and a reflector surface. The reflecting surface exists in various shapes and sizes depending on the intended applications. Besides some small telescopes with a reflector diameter of only a few meters, other ones use a reflector beyond 100 m. Most of the radio telescopes have an axially symmetric reflector [IJ07]. [CH69] states, that the most common shape is a paraboloid. It is formed by the rotation of a parabola around its vertical axis (say y-axis). Every cross section parallel to this axis delivers a parabola. The paraboloid of revolution is a special type of the elliptical one with the expression over the x-z-plane

$$y = a(x^2 + z^2) \tag{2.1}$$

The lowest point of the paraboloid and the origin of coordinates for equation (2.1) is called *vertex*. The rim of the reflector dish forms a plane parallel to the x-z-plane which is called *aperture plane*. [BHL+08][CH69]

Figure 2.1: Radio telescope Effelsberg[1]

A parabola, or in the three-dimensional case a paraboloid, is defined through a simple relation (see figure 2.2). For a parabola there exists a line perpendicular to the vertical axis with a point Q on it. This line crosses the vertical line at a point F. Then there could be any line parallel to the vertical axis crossing Q and a point P on the parabola. The sum of the length of this line and the distance from point P to F is constant. [Bal05] summarizes

$$\overline{QP} + \overline{PF} = \text{constant} = 2f \tag{2.2}$$

With this simple geometric construction and following Huygens' principle, it could be shown that incoming electromagnetic radiation as a plane wave always will converge in one focal point. This is located in the front face of the paraboloid. Every incoming bundle of rays parallel to the y-axis passes at first the aperture plane. Thereupon it reflects on the surface with an angle of incidence depending on the radius r from the y-axis. Then the radiation converges as a spherical wave towards the focal point. The intensities of the beams will sum up in this single point. The same characteristic could be described for the reciprocal direction: A source spreads a wave front in concentric spheres around the focal point. They impinge on the reflector plane and the surface reflects them. The paraboloidal dish then emerges the rays as parallel beams. This could be described as the feed "illuminates" the reflector plane. [CH69][Bal05][Baa07]

[1] "Effelsberg total2" by Dr. Schorsch - photo taken by Dr. Schorsch. Licensed under CC BY-SA 3.0 via Commons - https://commons.wikimedia.org/wiki/File:Effelsberg_total2.jpg#/media/File:Effelsberg_total2.jpg, 29.09.2015

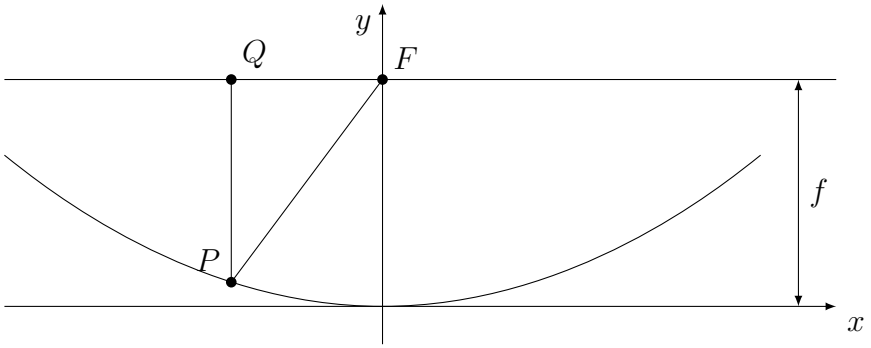

Figure 2.2: Definition of a parabola (similar to [Baa07])

The parameter a in the equation (2.1) is a measure for the curvature of the paraboloid and consequently the information about the focal distance. [Baa07] assumes

$$f = \frac{1}{4a} \tag{2.3}$$

as the corresponding point of focus on the vertical axis. The covered distance from the focal point to the aperture plane is called the path length and is constant for every beam.[BHL+08][CH69]

Antenna feed

In the focal point, a *feed antenna* absorbs the radiation. This is a device for receiving energy from the reflector. In this terms, the reflector is often referred as the *secondary antenna* while the receiving unit is the *primary feed*. Most of the radio telescopes are equipped with a pyramidal/conical horn or a dipole feed antenna. The feed antenna has to illuminate the whole reflector structure with a suitable (in ideal case uniform) distribution in phase and amplitude. It should not illuminate anything other than the reflector e.g. behind the rim. This is also called spillover and should be avoided. In such a case, it collects unwanted radio sources from the ground and sky to interfere with the intended radiation. [CH69][Bir11]

The primary feed is constructed to suit the secondary antenna. The intended application of the radio telescope dictates the type of the feed. There is a wide variety of antennas depending on objects like the frequency, bandwidth and polarization. An often used feed type are conical horns. Usually a horn is equipped with corrugations or ridges to meet the characteristics of the electro-magnetic radiation pattern. The size is determined by the frequency to measure. A lower frequency requires a bigger mechanical feed horn. Its design also depends on the ratio of focal length to diameter f/D. The aperture illumination as well as unwanted spillovers or a defocus are functions of this ratio. [IJ07][Imb11]

Support structure for the antenna feed

The support structure has to maintain a constant distance between the reflector surface and the primary antenna. The feed antenna of a front fed reflector is located directly in the path of the incoming rays. Hence itself and its support structure will shadow the reflector and produce unwanted scattering effects. Particularly the region of the strongest energy response in the middle of the reflector dish will be blocked. Normally the feed is supported by one up to four legs mounted on the backing structure of the reflector. These legs should be as small as possible to minimize the influence on the illumination and therewith the efficiency of the whole antenna. [CH69][RS07]

A possibility to avoid the blockage and scattering in the vertex region of the secondary antenna is an offset reflector. This is a non-symmetrical paraboloid with a focal point in a region of the aperture plane with a weaker field.[IJ07][Bir11]

The reflecting surface

An important characteristic of a radio telescope is the number of reflecting surfaces. A very fundamental design is the described parabolic reflector with the antenna feed located in the single focal point. This front–fed configuration is also referred as a prime-focus or single-aperture telescope. With a great reflector surface this is a convenient construction for large wavelengths in order to avoid major diffraction effects. For higher frequencies a dual–reflector design could be used. In this case a secondary reflector is located contrary in the path of rays between the original antenna feed and the reflector. This dual reflector systems come in two popular types in analogy to their optical pendants called Cassegrain and Gregorian telescope designs. Both keep their original reflector with a paraboloidal shape – now referred as *primary*. But the Cassegrain comes with a hyperboloidal and the Gregorian with an elliptical secondary reflector. For both, the incoming wave front reflects at first on the primary reflector and converges towards the surface of the second one. The new focal point is located in the region of the vertex point of the primary reflector. [IJ07][Bal05][Baa07]

In such a system the feed antenna and the electrical equipment can be placed behind the primary reflector. This is a great advantage because the heavy and bulky apparatus of the feed can be placed close to the strong backing structure. This implies a lower blockage in comparison to a single–reflector system. In addition the transmission line from and to the receiver is shorter than the way along the support stand. An additional electrical noise or a loss in the transmission wires may not be tolerable.[Bal05]

In contrast to the restriction for the primary feed, the reflector is normally suitable for a big range of wavelengths. The reflecting surface of a radio telescope is typically made out of metal (steel or aluminium) layers. The thickness of the panel is less important because of the small penetration depth of the incoming radiation. Hence it is mostly determined by the demanded mechanical stability. Usually the metal cover is formed by separate panels. A common solution is to mount them radial around the centre of

the paraboloid (vertex point). [CH69][BGS02][Bir11]

The reflector panels are mounted upon the backing structure. Hence, this support has to maintain the paraboloidal shape of the attached panels. Some telescopes like the Effelsberg Radio Telescope or the one in Green Bank are equipped with small linear actuators on the four corners of every surface panel. They are used to uphold the intended reflector shape and correct it in case of unwanted deviations. A common name for this is *active surface*. This is an exclusive infrastructure only used in a few telescope because of the expense. Other telescope mount the panels by screws to maintain an intended distance between the backing structure and the surface panels. They are adjustable by hand.[Kit90][IJ07][BGS02]

Actuation for the movement in azimuth and elevation

It is a common request to take into account an articulation of the telescope. In practice the antenna can be tiltable and rotatable so that its axis is able to point in any desired direction in the sky. The tilt from the horizon to the zenith is called *elevation* movement while the rotation around the vertical axis is referred as the *azimuth* direction.[CH69]

[Gaw04] assumes the movements as normally independent. Hence, they are considered as two single axis systems. [Kit90] presents various types of configurations of the actuation and mounts for the antenna itself. A typical system moves the whole telescope set–up in azimuth relative to the ground. On the top of the support stand a mechanism rotates the reflector dish with its component around a horizontal axis.[Kit90]

2.1.2 The INRAS RT-20 radio telescope

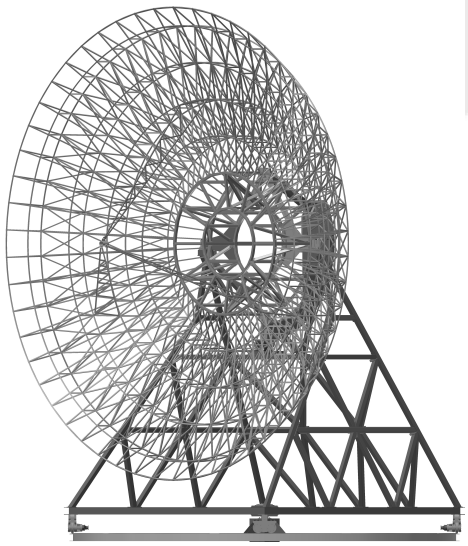

Figure 2.3: Backing structure and support stand of the INRAS RT-20 radio telescope

The mechanical part of the INRAS RT-20 radio telescope consists in general of a parabolic reflector, its supporting structure and the feed tripod. It is a front fed single-reflector system. The reflector surface is a symmetrical parabola following the equation

$$\begin{aligned} y &= a\left(x^2 + z^2\right) \\ &= 29.04\left(x^2 + z^2\right) \end{aligned} \tag{2.4}$$

with y as the vertical axis. With equation (2.4), the focal distance is [Baa07]

$$\begin{aligned} f &= \frac{1}{4a} \\ &= 7.260\,\mathrm{m} \end{aligned} \tag{2.5}$$

The diameter of the reflector surface is designed with 20 m. With the focal distance from equation (2.4), it will have a focal ratio $f/D = 0.363$.

Figure 2.3 shows the backing structure of the reflector dish. At this time the reflector surface has no final design yet. It is intended to lie upon the backing structure consisting of several trapezoidal–shaped panels. Every panel is attached to the reflector framework by adjustment screws as spacing elements. There will be in minimum four supports in every corner. They assure a proper mounting on the truss work. Furthermore it will be possible to set up the position of the surface panels by adjustment of the screws.

The antenna is able to perform an azimuthal movement around the vertical axis. The elevation angle goes from 10° to 95° as measured from the horizon and up. Most of the time the radio telescope will target at an angle of 55° to the sky.

The RT–20 will have a changeable antenna feed. There are several primary antennas with a variety in size and weight depending on the wavelength to measure. Today there are two sizes of feed horns and a dipole plate. One of the horns is designed for the use with a frequency of 10.65 GHz and the other for 1420 MHz. For the exchangeability this equipment should be easily accessible for a human. The tripod will be attached on two hinges on the lower two legs and a detachable connection on the upper one. With a mechanism of a motor and appendant gears it will be possible to lower down the tripod to access the feed horn.[HFA+14]

2.1.3 The surface accuracy as a measure for the antenna performance

The electrical performance of radio telescopes depends substantially on the surface accuracy. There are both systematic and random sources of imperfections. Some occur during production and installation of the surface panels. They may depart

from the ideal shape due to their mounting on discrete support points on the backing structure. This could force the panels into a plane or any other form instead of their intended curved profile. Other errors arise from environmental influences during the operation of the radio telescope. Deviations from the ideal shape result in a change of the path length and thereby cause variations of the phase characteristic of the waves. This ends in a loss in power at the primary feed. Hence, the reflecting surface should not depart significantly from its ideal paraboloidal shape. Even small aberrations from the ideal shape could reduce the antenna performance significantly.[Kit90][Lev94][CH69][UJJ+11]

The standard article concerning the gain loss as a function of the surface accuracy is written by Ruze in the year 1966 [Ruz66]. He assumes mostly random surface deviations due to environmental influences like gravity, wind and temperature. Bird summarizes in [Bir11] his derivation for the gain as

$$G = G_0 \mathrm{e}^{-(4\pi\epsilon/\lambda)^2} \tag{2.6}$$

G_0 denominates the gain of the undistorted reflector. ϵ is the root-mean-square error of the surface and λ the wavelength. Hence for a given wavelength but an increasing RMS error (RMSE) the antenna gain reduces.[Ruz66]

[CH69] found that the surface error ϵ corresponds to the maximum allowed phase error in the antenna feed which leads to the assumption

$$\epsilon = \lambda_{\min} \frac{1}{20} \tag{2.7}$$

with $\lambda_{\min}$ as the minimum wavelength to work with. A radio telescope is intended to work with a specific wavelength. Thus equation (2.7) sets a demand on the maximum tolerable surface deviation. With equation (2.6) and an assumed surface accuracy from (2.7), the antenna efficiency is $\approx 67\,\%$.[BGS02]

Ruze [Ruz66] assumes that the surface deviations δ_i for any discrete point i are values with a Gaussian distribution. For this case [KCC87] argues that the mean of the measured values is zero and so the standard deviation is equal to the root mean square. Following [BHL+08], the standard deviation or rather the root-mean-square is a quadratic mean and defined for a discrete distribution of n points as

$$y_{\mathrm{rms}} = \sqrt{\frac{1}{n} \sum_{i=1}^{n} y_i^2} \tag{2.8}$$

The root-mean-square error describes the deviation δ_i of a discrete point set from another. Thus it is a convenient way to express the error ϵ between an ideal surface and a deformed one with the aid of a set of discrete sampling points with the deviation

δ as [WD07] suggests:

$$\epsilon = \sqrt{\frac{1}{n}\sum_{i=1}^{n}\delta_i^2} \tag{2.9}$$

The deviation δ_i is defined and treated differently in the literature. Sometimes it is used to express the path length error [KCC87][Kat70]. Other publications use the deviation in the axial direction like in [WD07].

2.2 Deforming environmental influences and their estimation

2.2.1 Natural limitations to the reflector design

In the year 1967, VON HOERNER proposed in [Hoe67a, Hoe67b] three natural limits for the diameter of the reflector and the shortest wavelength to observe. Due to the *stress limit* it is not possible to built infinitely high structures. A limit is reached when the weight of the structure induces a pressure equal to the maximum stress in the material. Assuming S as the maximum allowed stress of the material, ρ as the density and a γ as the geometrical shape factor, the maximum height of the structure is $h_0 = {}^{\gamma S}/_{\rho}$. This is the compression of a structure under its own weight. [Hoe67b] suggests a stress limit for the diameter of a steerable telescope of

$$D \leq D_{\mathrm{st}} = 600\,\mathrm{m} \tag{2.10}$$

The *thermal limit* restricts the minimum wavelength for the reflector. Due to a gradient in temperature, parts of the reflector structure will elongate through thermal extension. This leads to a deflection of the whole structure and therefore to a loss in surface accuracy. [Hoe67b] proposes a critical minimum wavelength as

$$\lambda \geq \lambda_{\mathrm{th}} = 2.4\,\mathrm{cm}\frac{D}{100\,\mathrm{m}} \tag{2.11}$$

The possibility to tilt a reflector structure with a given dead weight causes the *gravitational limit*. The deflection of the surface sets a restraint to the minimum wavelength as [Hoe67b] predicted with

$$\lambda \geq \lambda_{\mathrm{gr}} = 8.0\,\mathrm{cm}\left(\frac{D}{100\,\mathrm{m}}\right)^2 \tag{2.12}$$

The resistance to deformation increases with the square of the size while the weight grows with the third power.[HW75]

All three limits arise from deformations of the reflector structure. A free-standing telescope is exposed to gravitational and wind forces as well as differential thermal expansion. As the gravitational deformations are the largest effects a suitable structural design may allow to reduce them.[BGS02]

2.2.2 Gravitational influence on the reflector structure

The described stress limit in section 2.2.1 restricts the diameter of a radio telescope to about 600 m. Especially for tiltable telescopes the gravitational limit is reached much earlier. [BGS02] assumes this restriction to be the main environmental influence. Tiltable radio telescopes are exposed to recurring changes in the direction of gravity forces. Since the construction is designed with a finite stiffness, it will deform under its dead weight.[HW75]

Kitsuregawa [Kit90] claims three main modes of dead weight deformation:

- those causing displacement and rotation of the reflector relative to a fixed coordinate system
- those causing change of the focal length of the reflector
- those causing a departure from the paraboloidal shape of the reflector

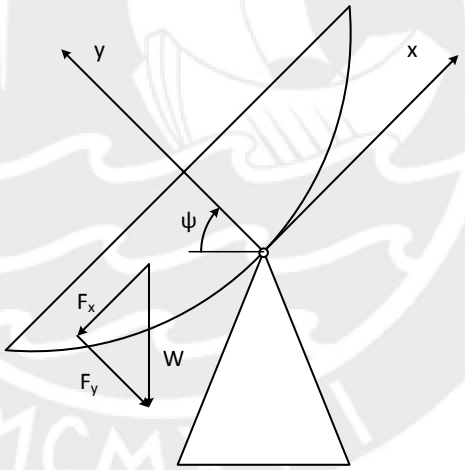

Figure 2.4: Components of gravity acting on a reflector assembly with W as the dead weight and ψ as the elevation angle [Kit90]

While the antenna is rotating around the elevation axis the direction of the force due gravity changes. The force is a function of the elevation angle ψ. [Kit90] splits the acting dead weight into the axial and the radial load:

$$F_{\mathrm{x}} = -W\cos(\psi) \tag{2.13}$$

$$F_{\mathrm{y}} = -W\sin(\psi) \tag{2.14}$$

For the static analysis it is assumed that the distortion of the reflector assembly is linear.[WD07] Expecting this, the displacement of the structure nodes is proportional to the gravity loading. [HW75] shows with Hooke's law that

$$\Delta \boldsymbol{y} = \boldsymbol{K}^{-1}\boldsymbol{F} \tag{2.15}$$

$$\begin{pmatrix} \Delta y_1 \\ \vdots \\ \Delta y_n \end{pmatrix} = \boldsymbol{K}^{-1} \begin{pmatrix} F_1 \\ \vdots \\ \mathrm{F}_n \end{pmatrix} \tag{2.16}$$

where $\Delta \boldsymbol{y}$ is the displacement vector parallel to the optical axis of the discrete node points in the reflector structure. $\boldsymbol{K}$ is the matrix of the stiffness containing information about the distribution of elements, the shape size, the position in space, the type of material and other conditions. $\boldsymbol{F}$ is the force vector in the direction of gravity with

$$\begin{aligned} F &= F_{\mathrm{x}} + F_{\mathrm{y}} \\ &= W\cos(\psi) + W\sin(\psi) \end{aligned} \tag{2.17}$$

containing the two components from the equations (2.13) and (2.14). [HW75] [WD07]

The deformation vectors $\boldsymbol{\delta}_0$ and $\boldsymbol{\delta}_{90}$ for the face-side (elevation $\psi = 90°$) and the face-up (elevation $\psi = 90°$) situations are constant. $\boldsymbol{\delta}_0$ is the deformation vector normal to the surface when the gravitation is applied in the direction $-x$. Accordingly $\boldsymbol{\delta}_{90}$ is the deformation vector for a gravity load applied in $-y$-direction. Because of the assumed linear behaviour, it is possible to determine any intermediate state between them. [HW75] [WD07] The deformation vector as a function of elevation angle ψ can be derived by superposition as

$$\boldsymbol{\delta}(\psi) = \boldsymbol{\delta}_0 \cos\psi + \boldsymbol{\delta}_{90}\sin\psi \tag{2.18}$$

A possibility to handle the dead weight deflection was introduced by VON HOERNER in the year 1967. His method is called *homology design* and will be described in section 2.3.1.

2.2.3 Wind forces on the reflector structure

[Kit90] refers to three sets of wind conditions for a radio telescope: operational wind velocity, steerable wind velocity and survival wind velocity. Up to the operational velocity the antenna meets the required performance specifications. To avoid operating under a higher wind velocity, normally a statistical long-term wind analysis would be done to provide a reasonable availability of the radio telescope. In case of a high wind velocity the telescope could be driven to a rest position and may be locked. For a exceptionally higher wind velocity the antenna would be driven into the minimum stress position, at zenith.[Kit90]

[FHY+13] calculates the wind load for the INRAS RT-20 based on the norm "ASCE 7 - Minimum design loads for buildings and other structures, 2006" [ASC06]. [FHY+13]

concerns about the mechanical resistance to environmental loads. Hence, it contains an approach to determine an overall maximum wind force on the reflector dish and aims at proving the mechanical stability of the telescope construction. [FHY+13] uses the equation for wind loads on open buildings from [ASC06]. With a dynamical pressure q_z, the gust effect factor W_G, net force coefficients C_f (see [ASC06]) and A_f as the projected area normal to the wind, the wind force can be expressed as

$$F = q_\mathrm{z} W_\mathrm{G} C_\mathrm{f} A_\mathrm{f} \tag{2.19}$$

The dynamical pressure q_z is calculated in [FHY+13] with the specific environmental conditions for the city of Lima. With equation (2.19) a single value for the wind load of the RT-20 can be found. This force applies on the bars of the reflector backing structure.

[VSA04],[UJJ12a] and [UJJ13] describe a straight numerical way. To study the influence of wind forces on the reflector of the VIRAC RT-32 finite element simulations on a simplified geometry are used. This work uses the reflector surface as a model for the Computational-Fluid-Dynamic (CFD) simulation and a beam-based model of the backing structure for the calculation of the wind induced deformations. The reflector surface is modelled as a finite volume divided in rectangular parts. It will be exposed to a wind flow as a compressive load.[UJJ12a]

[UJJ12a] expects a turbulent flow around the radio telescope because of the dimensions of the antenna and the wind speed. Therefore only turbulence models like the Reynolds Averaged Navier-Stokes (RANS) and the Large-Eddy Simulations (LES) are used.

The wind induced deformation depends on the direction of the wind. Therefore [UJJ12a] studies various situations while changing the elevation angle as well as the wind direction. The calculations of [UJJ12a] show that the wind induced deformations are small in comparison to the gravitational load.

2.2.4 Thermal influences on the reflector surface

Beyond the gravitational limit, an important problem for the operation of a radio telescope is the temperature. A large antenna normally is built in the open. Through sunlight and the corresponding shadow, a temperature gradient ΔT arises. It is independent from the reflector diameter but it induces deflection as a function of the diameter D. The deflections will increase linearly with a growing D. A comparison of the gravitational limitation from equation (2.12) and the thermal restriction of (2.11) shows the changing importance of both as a function of the diameter. For smaller antennas the thermal restriction demands a higher wavelength than the gravity limit. With increasing diameter the gravitational influence produces more effect. For the given values the turn-over is reached for a diameter of approximately 30 m. [Hoe67a]

[BSGN04]

The deflection due to an absolute temperature of a panel made of one material is very small. [HEH89] found a variation of $4\,\mu$m for a temperature change of 20 K. Much more potent is a heat gradient. [HEH89]

As the temperature is induced through sunlight the effect is negligible at night or on cloudy days. Furthermore even on sunny days a reflecting paint at the surface panels could reduce the thermal gradient. [Hoe67a] found for Green Bank, West Virginia a difference of the temperature between the metal surface in sunshine and the backing structure in the shadow of 8 K. A common value for the temperature gradient is assumed to $\Delta T = 5\,\mathrm{K}$. The temperature and so the influences are changing very slowly in comparison with wind or gravitational forces.[Baa07]

A radome or something similar is a possibility to protect the reflector surface from solar influence. The James Clerk Maxwell Telescope [HEH89] uses a housing to keep the air temperature from increasing too much. The outside of the building is painted white and the inside surface as well as the structure of the telescope is covered with metal reducing the thermal radiation. With this arrangements [HEH89] measures variations under 1 °C.

2.2.5 Estimation of reflector deformation by finite element methods

A method to determine surface deviations due to dead weight was suggested in section 2.2.2 and will be continued in 2.3.1. Assuming the linearity of the gravity deformation, this principle of superposition delivers a proper solution. This was the first finite element solution for that problem invented by Hoerner for his homology design method [Hoe67a].

Much more often a solution with a ready for use FEM-software can be found. [WD07] compares both superposition and the solution of a structural analysis using the FEM-Software ANSYS. The software uses a structural model to represent the physical and mechanical characteristics of the telescope structure. Information about the dead weight or rather the gravity, wind and thermal loads are inputs of the software. The software solves the mechanical problem in a numerical way for a given load situation on the mechanical model. The simulation delivers corresponding displacement vectors (or maybe forces) of discrete points in the structure. Often, the resulting deformed structure shape can be displayed in the software environment directly.[Kit90][Baa07]

Often, only the reflector backing structure or some parts directly attached to this (like the surface panels or a counterweight) are imported to the FEM model (compare [WD07][Kit90][BSGN04] and others.) The truss work structure of the telescope can be modelled as beam elements with a defined geometry and mechanical properties

2.2.6 Estimation of reflector deformation by measurements

A very common method to determine the deformation of the reflector surface are measurements on the real telescope. The methods use the information about displacements of discrete points upon the reflector surface. This can be done by optical telemetry. Objects to measure are angles as well as ranges depending on the applied method. [ZZY+12] describes an angle metrology system for the 65m-Nanjing-telescope with an active surface. Their method uses a laser in combination with photosensitive CCD camera sensors.

[BBI02] is pointing with a theodolite at 367 small tape targets on the reflector surface. They are spread radial all around the paraboloid. The measuring instrument is placed in the vertex of the paraboloidal dish. From this position the theodolite measures both distances and angles to every target point on the reflector.

Another example are photogrammetric measurements like in [Sub05]. The Cassegrain system of the Australia Telescope Compact Array was measured by photographies of reflective targets of the reflector surface.

Beside them, there are other methods like the interferometric approach of a radio holography measurement (compare [KL13] and [LAMV04]).

2.3 Compensation of recurring reflector surface deformations

2.3.1 Surpassing the gravitational limit using the homologous design method

There is a trade-off to solve in the design phase of a reflector. To capture most of the feed energy, a reflector ought to have an aperture plane as large as possible. On the other hand, the size is limited by mechanics because of the deflection under its own weight. The first radio telescopes until the 1960s are designed to provide a sufficient stiffness against any deformation. Their rigidity was intended to assure an invariable shape of the reflector surface independent from external influences. This approach is implementable until a critical size of the reflector diameter (compare section 2.2.2). Only an ideal antenna provides infinite stiffness. The increase of size and simultaneously the demand on a high surface accuracy were provoking a limit in economical and technical regards.[Baa07]

[Hoe67a] proposes four possibilities to pass by this gravitational limit:

- use a fixed elevation transit telescope
- motors in the surface panels to remediate the deformations

- counterweights with levers like in optical telescopes to annihilate deformations
- allowing those deformations that do not reduce the electric performance

All of them were applied in several telescope designs. But [Hoe67a] prefers the last one as the most natural one. The construction will be allowed to deform under its own weight as a function of the elevation angle. But for any direction of the gravity vector the reflector dish will transform conformally from one surface shape to another one of the same type. Hence, a reflector with a parabolic cross section will always retain in a paraboloidal shape. This characteristic is called *homologous deformation*. For such deflections only the focal length and the position in space will change. The parameters to describe the homologous deformed paraboloid are also called *homology parameters*. [Hoe67a]

The homology design method was developed by VON HOERNER in the year 1967 [Hoe67a]. The former radio telescope used a conventional truss work design consisting of a main frame made by heavy square boxes with a higher stiffness than the rest. Such a structure deforms in a non-uniform way. For the method of VON HOERNER this is an unwanted behaviour. An homologous deformation requires an equal stiffness of each surface point. [Hoe67a] notes that its reasonable to change hard points into soft ones and obtain an overall "softness". This can be provided in a structure where the way from each point of the surface to the next bearing has the same length. An homologous deformation can be demanded for any number n of points. Then n should be chosen in such a way that any deformation between neighbouring points can be neglected. [Hoe67b] recommends

$$n = 3\frac{\lambda_{\mathrm{gr}}}{\lambda} \tag{2.20}$$

where λ_{gr} is the critical wave length due to gravitational deformations (see also section 2.2.2).

The constraint of equal distances and high symmetry (compare [HEH89]) gives the geometrical input for the approach described by VON HOERNER in [Hoe67b]. Thereupon, he derives an algorithm to calculate suitable bar areas for the reflector backing structure to obtain an homologous design. The method uses the ideas of the gravitational deformation shown in section 2.2.2. The assumption of linearity gives two deformation vectors $\boldsymbol{\delta}_0$ and $\boldsymbol{\delta}_{90}$ for the face-down and face-up position of the reflector dish. With the equation (2.15) derived from HOOKE's law, they contain the information about stiffness and geometry (the force F implies the gravity vector as well as the geometrical and material properties). [Hoe67b] defines

$$\Delta H = \sqrt{\frac{1}{2n}\sum_{i=1}^{n}\delta_{0,i}^2 + \sum_{i=1}^{n}\delta_{90,i}^2} \tag{2.21}$$

as the deviation from homology. The variables $\delta_{0,i}$ and $\delta_{90,i}$ represent the difference between the deformed surface point i and the corresponding point on the best fitting

paraboloid of revolution:

$$\delta_{0,i} = \Delta y_{0,i} - \Delta y_{b,i} \tag{2.22}$$

$$\delta_{90,i} = \Delta y_{90,i} - \Delta y_{b,i} \tag{2.23}$$

The method now searches for beam areas to minimize the deviation ΔH. Equation (2.21) needs initial values for all bar areas. These are estimated by assuming a structure that withstands the fundamental survival conditions. All bar areas change simultaneously at each iteration step.[Hoe67b]

2.3.2 Determining a geometrical description for the distorted reflector surface

Identification and parameters for a best fitting surface function

With the applied loads like gravity, wind and a temperature gradient, the reflector surface will not be identical to the theoretical design. It will be deflected and changed in its shape. An analysis of the reflector distortion allows an estimation of the achievable surface accuracy and therewith a prediction of the feasible antenna performance (compare section 2.1.3). Furthermore, the examination of the deformed reflector dish could deliver a geometrical description of the actual surface. Then, a mathematical function allows a prevision of the expected relative shift between the focal point of the new distorted paraboloid and the position of the primary feed antenna. While the most common type of reflector shapes is the axial symmetric paraboloid (compare [IJ07]), this section will treat the identification of a best fitting paraboloidal function.

A paraboloid in space is defined by six parameters. [Baa07] proposes to extract the information about the paraboloidal shape of the deformed reflector from the FEM-data. The FEM delivers a data set of cartesian coordinates in a three-dimensional space for the reflector. For this point cloud, it may be possible to determine the location and orientation of a paraboloid that fits best. Six parameters could characterize a paraboloidal plane:

- 3 cartesian coordinates of the reflector vertex (x,y,z)
- 2 angles for the rotation around the x- and y-axis (ϕ_x, ϕ_y)
- the focal length f

The usual approach for finding the best fitting paraboloid consists of the determination of these 6 parameters. It is not required that the shape of these parameters would fit the data set of coordinates perfectly while this is an approximation. There may be a residual fitting error. The parameters can be found by minimizing the rms surface error of the path length or the deviation in the vertical y-direction (2.9).[WDQ+04]

Approximation of the best fitting function

The method of finding a best fitting function respectively a paraboloid for the reflector uses discrete nodes distributed over the surface. Over these sampling points a function has to be found that fits every node as much as possible. The displacement of each node is divided in two parts: one is the rigid motion described in the previous section 2.3.2. The other is the residual deviation of all nodes from the new function.[WDQ+04] As the deformed surface is close to an ideal parabolic shape for every deformation, there is a paraboloid that fits best. From the idea of the root-mean-square error as a description of the surface deviation (compare equation (2.9)), [HW75] defines

$$\epsilon_{\psi}^2 = \frac{1}{n}\sum_{i=1}^{n}(\Delta y_i - \Delta y_{\mathrm{b}i})^2 \tag{2.24}$$

as the deviation of the actual (deformed) surface from a best fitting paraboloid. Δy indicates the displacement vector in y-direction. Δy_b refers to the corresponding y-value of the best-fit paraboloid.[Hoe67b][HW75]

The best-fit-paraboloid can be found by minimizing the surface error ϵ_{ψ}. [WD07] and others use this least-square method to fit a paraboloid with six parameters. A usual form is the interpretation of the reflector-function as a paraboloid shifted and rotated in space with a change in the focal length. [WD07] assumes

$$y_i^* = y_i - \frac{x_i}{2f}u + v - \frac{z_i}{2f}w + z_i\phi_{\mathrm{x}} - x_i\phi_{\mathrm{z}} + \frac{y_i}{f}h \tag{2.25}$$

as a suitable equation to determine the points of the new paraboloid (with vertical axis value y_i^*) based on the theoretical (undeformed) surface (y_i-values). [WD07] uses u,v,w as the variables for the translational shift of the vertex. ϕ_x and ϕ_z are the angles to express the rotation around the correspondent axes. The parameter h stands for the focal shift.

CHAPTER 3

Task specification and requirements

The object of this thesis is to create a design for a mechatronic actuator to adjust the primary antenna of the INRAS RT-20 radio telescope. This actuator should help to compensate a misalignment between the focal point of the reflector surface and the actual position of the primary antenna due to deformations of the reflector structure.

The literature offers a wide range of approaches and methods for the analysis of various types of reflector deformations. These are mostly specific solution for individual radio telescopes. Hence the actual work has to clear the way for a suitable analysis of the surrounding conditions for the RT-20. At first it is necessary to get informations about the expected deformations. The main influence to analyse is the deformation due to gravitational impact. Other environmental influences like wind loads and deflections caused by thermal expansion of the materials will not be subject of the examination. The wind forces are expected to be small at the designated site. Furthermore the absence of a final design of the reflector surface allows no suitable simulation of neither the wind load nor the temperature induced deformations.

The expected deformations of the telescope affect the structure and the surface of the reflector construction. A possibility to estimate the induced deformations is a computational numerical analysis. A model of the telescope structures or parts of it will be set into a FE-(Finite Element)-simulation software. The software is able to compute the reactions to induced forces of a given mechanical structure with known geometry and material properties in a numerical way. The result of this simulation is the information about the deformed structure model. The actual work requires the information about the displacement of discrete points forming the reflector surface.

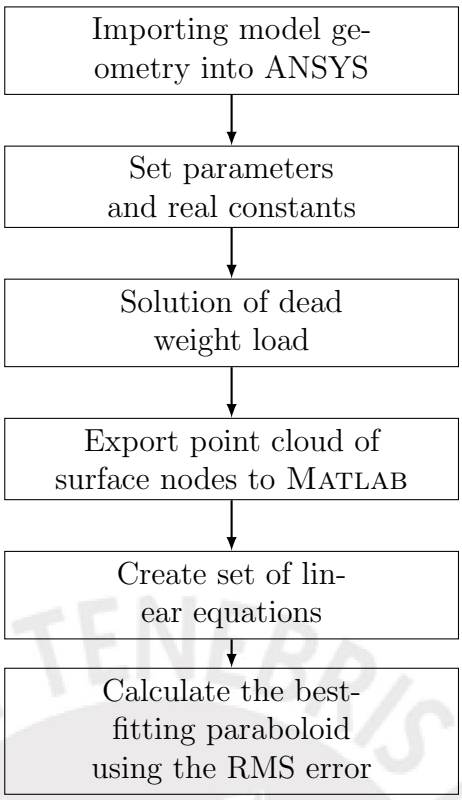

Figure 3.1: Software sequence for the deformation analysis

An important idea during the process of construction of the RT-20 radio telescope was the homologous design. This concept refers to an uniform deformation of the reflector backing structure. It allows a transformation of the reflector surface but always preserving its paraboloidal shape. So even the distorted reflector surface is assumed to be a paraboloid. That means at the same times the reflector keeps a focal point even though its position may have changed. This is the basic requirement to be able to refocus the telescope. With the knowledge of the characteristics of the new paraboloid, it is possible to calculate the position of the new focal point.

The necessary result of the simulation process is a data set of coordinates in space forming the reflector surface. Assuming a homologous deformation there exists a paraboloid that best fits this point cloud. The calculation of this could be done determining the paraboloid with the smallest root-mean-square error to the coordinates of the simulation data set. For the identified paraboloid the corresponding focal point can be computed.

The anticipated software-related workflow is shown in figure 3.1. Entering the sequence the complete CAD-Model is expected. The last step of the process is designated to deliver a mathematical description of the actual paraboloid and therewith the location of the new focal point.

The second part of the thesis consists of the design process of the feed actuator itself. The functional requirements are given through the usage purposes of the future radio telescope. The environmental conditions have to be evaluated and analysed. For a proper mechatronical design process, different suitable solutions (also particular solutions) have to be developed and evaluated. At the end one concept will be elected for further work.

CHAPTER 4

Determination of the focal shift for the INRAS RT-20

4.1 Simulation of deformations for the reflector structure with FE-Software ANSYS

4.1.1 Modelling of the telescope structure

The original design of the RT–20 telescope structure was done in the institute for radio astronomy by Heraud and then structurally calculated by Zegarra of the civil engineering department. The final structural model was contracted with the INACOM group of the PUCP Lima [FHY+13]. The model of the telescope (figure 4.1) includes the support stand and the reflector structure with tripod as well as the counter weight and actuators to perform the azimuth- and elevation-movements.

This model is the basis for the finite-element analysis of the deformation. The simulations are intended to obtain information about the deformation of the reflector surface with respect to its backing structure. Therefore the simulations have to affect in particular this part of the telescope. To simplify the simulation model, the support stand is assumed to be a fixed fundament without any deformation due to wind loads, temperature gradients or dead weight. Hence the lower part (the support stand) could be neglected, as long as it does not affect the behaviour of the reflector structure itself. In this case the antenna backing structure can be treated as detached and the suspension will be replaced by a fixation to the base on the original mounting points.

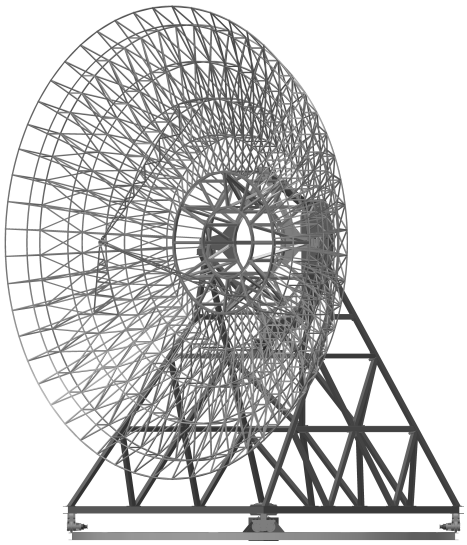

Figure 4.1: AutoDesk Inventor Model of the frame work for the radio telescope (with support stand, antenna backing structure and tripod)

The calculation in ANSYS is a structural analysis. This type of simulation is working with a line model for the description of the geometry. For a proper input into the simulation software the CAD–model from figure 4.1 is converted into a line model out of keypoints and lines like in figure 4.2.[MG07]

The model needs to have a fixation to the ground. In this model the support stand is already omitted. The backing structure was attached to the support stand via its frame bars. In the line model these bars were converted into two-dimensional lines. Hence the former mounting bars persist in form of the line arrangement in figure 4.3b. ANSYS provides the possibility to declare some elements as fixed to the ground restricted to neither a translational nor a rotational displacement. Thus the former mounting parts will be declared as base elements.[MG07]

The line model of the reflector backing structure is split into two parts. The inner *core* is designed with different framework bars as the *reflector plate*. Additionally the model contains the *tripod* for the antenna feed. It does not include the reflector surface with its aluminium panels.

Geometric properties of the frame work bars

The lines of the framework can be meshed with uni-axial beam-elements. These elements are able to represent a suitable behaviour to compression and tension as well as bending stress. The element connects two nodes and permits a DOF of three at every node: two translations and one rotation. For the present structure, BEAM188–elements are used. This type allows to define an arbitrary cross section for a beam bar. are Two types of profile sections were used in the whole structure. The core is

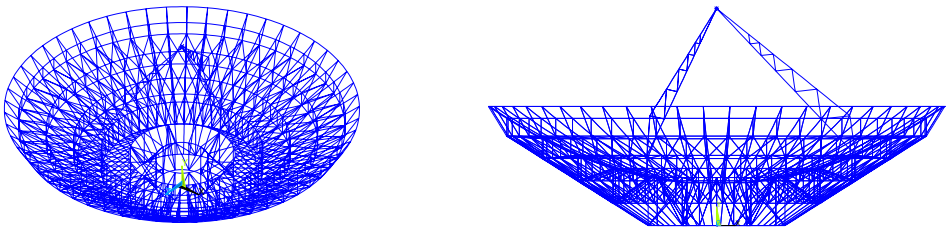

Figure 4.2: Reflector backing structure with tripod as line models

(a) Mounting of the antenna with attached counterbalance

(b) Lines on the backing structure defined as fixed base

Figure 4.3: Mounting of antenna backing structure. To replace the rigid mount a set of lines is defined as a fixed base

intended to be more rigid than the plate framework. To provide this, the core part consists of profiles with a higher section modulus. Figure 4.4 shows both. The profiles of the reflector plate have a quadratic section with a length of $B_\mathrm{p} = L_\mathrm{p} = 50\,\mathrm{mm}$ with B as the width and L as the height and according to

$$W_\mathrm{B} = \frac{BL^3 - bl^3}{6L} \tag{4.1}$$

the resistance of the plate $W_\mathrm{B,p} = 3138.61\,\mathrm{mm}^3$ is less than the $W_\mathrm{B,c} = 49\,210\,\mathrm{mm}^3$ of the core. [MG07][Lue10]

For the simulation the reflector core structure will be equipped with beams of the cross section with higher stiffness (figure 4.4b) and the outer reflector plate with the smaller sections from figure 4.4a

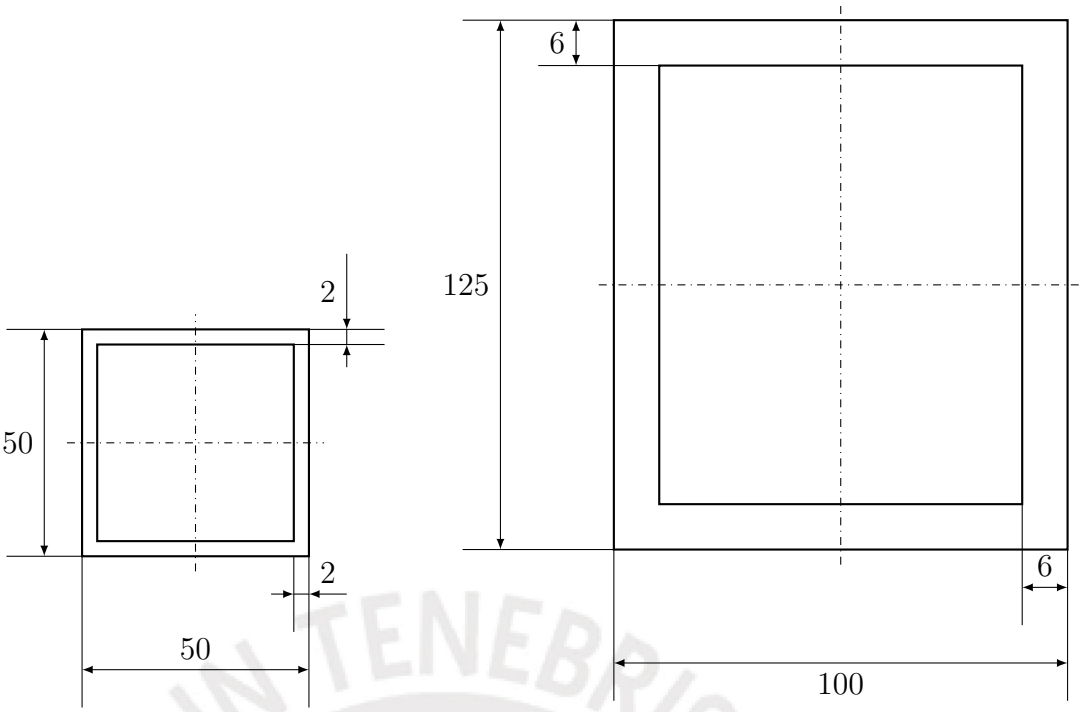

(a) section of plate profiles (b) section of core profiles

Figure 4.4: Profile sections in reflector frame work

Material

All framework bars are made of steel produced and donated by *Aceros Arequipa*. Table 4.1 shows the applied material parameters for the frame work bars. These values are provided by an internal publication made by the INACOM group of the PUCP Lima and will be used for the simulation.

parameter	unit	value
density	g/m^3	7850
modulus of elasticity	N/m^2	$2.0 \cdot 10^{11}$
poisson ratio	-	0.3

Table 4.1: Material parameters for the reflector backing structure

Mass of the future antenna feed

To consider the future mass of the primary antenna feed, a mass-element will be located on the top of the tripod-structure. The converging point of the three tripod legs represent approximately the mounting point of the feed horn. This will give an

adequate model to consider the feed mass and the equipment. The simulation software ANSYS provides an element named MASS21 to attach a virtual mass to a structure node.

Reflector surface

The presented Inventor-model does not include the reflector surface. Due to the fact that the INRAS RT-20 is still in development there is no established design available. Therefore this work has to deal with several assumptions about the future construction. Like mentioned in section 2.1.2 the reflector surface consists of several trapezoidal tile-shaped aluminium panels with double curvature (curved surface). Every panel is attached to 4 support points. As shown in figure 4.5 there are spacing pieces between the supporting points in the frame work bars and a surface panel (see also section 2.1.1). These spacers are manually adjustable to tilt and bend every surface panel to fit into the ideal paraboloidal shape.

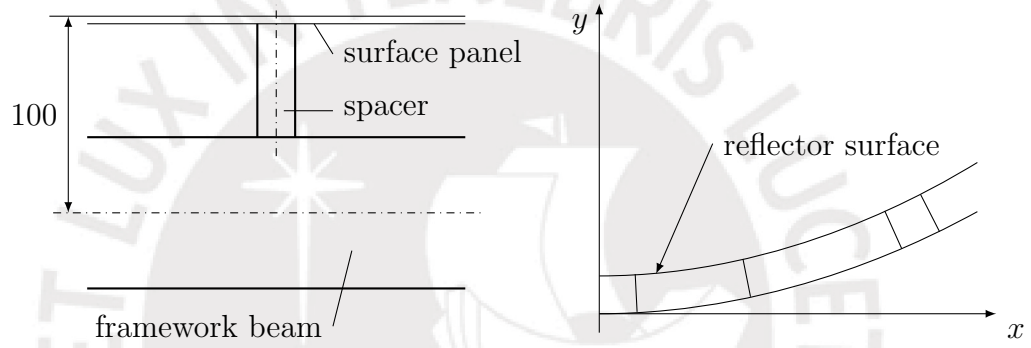

(a) Mounting of a surface panel on a frame work beam (detail)

(b) Exemplary points for support of the surface panels in y–x–plane

Figure 4.5: Spacer between frame work bars and reflector surface panels

For the ANSYS simulation, the surface panels as well as the spacer, will be neglected completely. Hence the simulation can not take into account a deformation of the surface directly. Instead of measuring a displacement of points in the surface, only movements of the underlying frame work will be considered. The connection between one frame work bar and the corresponding mounting point on a surface panel is supposed to be rigid. So there is no movement between them. A first assumption is to equate a displacement of both mounting points (bar and panel). The second one is to imply the same paraboloidal function for the reflector surface and the underlying bar structure. The last one is relatively easy to prove if a constant distance between them is provided.

The underlying beams form over the points of support for the adjusting screws a nearly parabolic function alike the future reflector surface. Because of the constant vertical distance (y–direction), it will be a equidistant plane. That means every tangential plane of this function is parallel to another on the surface paraboloid.[Bär13] The

	pt	$\sqrt{1+p^2t^2}$	$pt/\sqrt{1+p^2t^2}$	$1/\sqrt{1+p^2t^2}$
$t = 0.1$	0.0034	1	0.0034	1
$t = 10$	0.3444	1.0576	0.3256	0.9455

Table 4.2: Numeric results of terms from equations (4.3) and (4.4) for $p = 1/29.04$

fact of the non–existence of an equidistant paraboloid leads to new functional relation. A function with a distance d to a 2-dimensional parabola $y(x) = px^2$ could be parametrized as

$$\begin{pmatrix} x \\ y \end{pmatrix} = \begin{pmatrix} t \\ pt^2 \end{pmatrix} - \underbrace{\frac{d}{\sqrt{1+p^2t^2}} \begin{pmatrix} -pt \\ 1 \end{pmatrix}}_{\text{the normal (normalized) with distance } d} \tag{4.2}$$

and divided into the following components:

$$x(t) = t + \frac{dpt}{\sqrt{1+p^2t^2}} \tag{4.3}$$

$$y(t) = pt^2 - \frac{d}{\sqrt{1+p^2t^2}} \tag{4.4}$$

According to table 4.2 and for a distance $d = 0.1$, the x–component could assumed as

$$x(t) \approx t \tag{4.5}$$

The y-component also remains nearly with the constant offset d so that

$$y(t) \approx pt^2 - d \tag{4.6}$$

For this approximation for a equidistant 2–dimensional parabola, the functional relation only contains the constant offset d.

$$y(x) = px^2 - d \tag{4.7}$$

For further work, this argumentation is also applied to the 3–dimensional problem of an equidistant plane.

4.1.2 Simulation of gravity induced deformation

The deformation by gravity occurs due to the dead weight of the telescope (compare section 2.2.2). The line model of the telescope meshed with the geometry of the profile sections and the corresponding material parameters delivers the information about the magnitude and the distribution of mass in the structure. The weight of the telescope can be calculated by adding the information about gravity. For this issue ANSYS

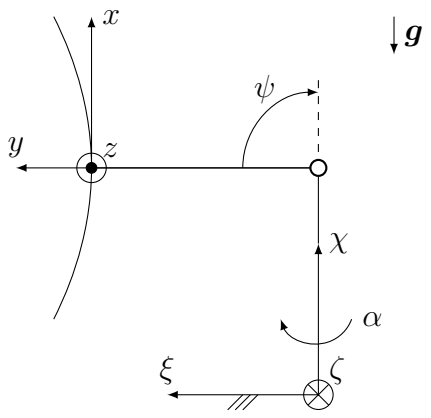

Figure 4.6: Coordinate systems on the radio telescope RT-20

provides a function to add an acceleration vector to a model.

In operation, the radio telescope will be able to change its elevation angle between 10° and 90°. Hence the impact of the gravitation vector $\boldsymbol{g} = (g_x, g_y, g_z)^T$ on the antenna structure changes as a function of the elevation angle ψ:

$$g_{\mathrm{x}} = -9.806 \cos\left(\frac{2\pi}{360}\psi\right) \frac{\mathrm{m}}{\mathrm{s}^2} \tag{4.8}$$

$$g_{\mathrm{y}} = -9.806 \sin\left(\frac{2\pi}{360}\psi\right) \frac{\mathrm{m}}{\mathrm{s}^2} \tag{4.9}$$

$$g_{\mathrm{z}} = 0 \tag{4.10}$$

The simulation will be done as a series of increasing elevation angles from 10° to 90°

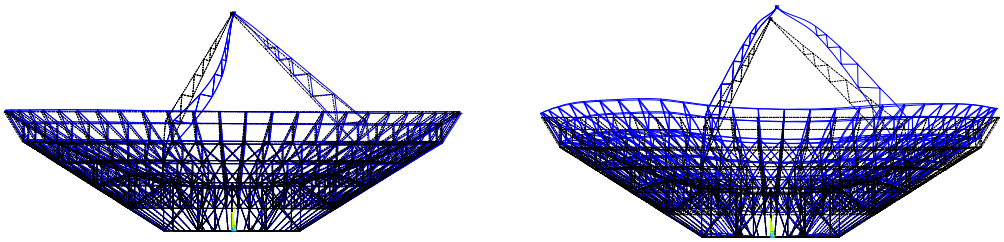

(a) $\psi = 10\,^\circ$ (b) $\psi = 90\,^\circ$

Figure 4.7: Deformed (blue) in comparison to the undeformed structure plotted in ANSYS for two elevation angles (exaggerated)

in steps of 5. Figure 4.7 shows exemplary two load situations and the deformed model in comparison to the original one.

4.1.3 Definition of the output of the ANSYS-Simulation

The ANSYS-Simulation is designed to deliver the information about the displacement of nodes composing the reflector surface. As mentioned in 4.1.1, it is not possible to determine the displacement of the surface nodes directly. Only the movement of the underlying nodes of the backing structure on the support points could be identified. Figure 4.8 shows an imaginable selection for suitable support points. For further work, these points will be treated as the actual real reflector surface (compare 4.1.1).
For the selected points the original coordinates or rather the position vector $\boldsymbol{v}_i$ as well

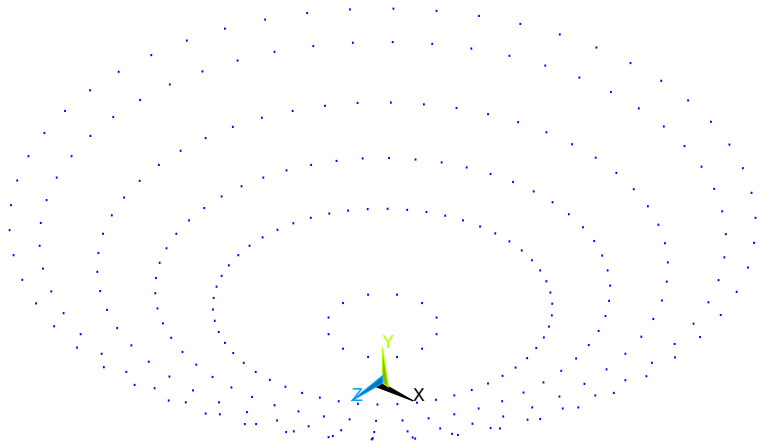

Figure 4.8: Selected supporting points for the surface (assumption) displayed in ANSYS APDL

as the displacement vectors $\boldsymbol{d}_i$ will be exported into a text file. Because the following calculation is about the determination of the new focal point of the paraboloid, the displacement of the antenna feed is in the same way important. Therefore, the original coordinates and the displacement of the node with the attached MASS21–element will be contemplated as well.

In summary the written scripts instruct ANSYS to run several simulations. For each solution text files for the

- coordinates of the undeformed surface nodes
- displacement vectors of surface nodes
- coordinates of the reference focal point
- displacement vector of focal point

are created.

4.2 Identification of a Best-Fit-Paraboloid (BFP) for the deformed reflector surface

The numerical solution in ANSYS delivers a displacement vector $\boldsymbol{d}_i$ for every node i. With this information and the original coordinate vector $\boldsymbol{v}_i$, the new position $\boldsymbol{v}_i^*$ of every node in the deformed state could be easily calculated:

$$\boldsymbol{v}_i^* = \boldsymbol{v}_i + \boldsymbol{d_i} = \begin{pmatrix} x_i \\ y_i \\ z_i \end{pmatrix} + \begin{pmatrix} d_{x,i} \\ d_{y,i} \\ d_{z,i} \end{pmatrix} \tag{4.11}$$

The data set of node coordinates in a three-dimensional space is a point cloud out of nodes of the actual surface (compare figure 4.9 for a 2–dimensional equivalent). The theoretical surface is the reflector plane in original undeformed state. According to the design this surface follows

$$y(x,z) = \frac{1}{29.04}x^2 + \frac{1}{29.04}z^2 \tag{4.12}$$

The discrete result of the deformation analysis in ANSYS is the displacement matrix for the surface nodes.

Assuming to have a paraboloidal shape of this point cloud, a best fitting function y^* could be found minimizing the RMS (root mean square) error (see equation (2.9)) of the vertical residuals between the calculated surface points and the best-fitting plane. Another suitable and frequently used method is the minimization of the pathlength error as the distance between a surface point and the focal point. The former method will be used.

[WD07] uses an equation with six fitting parameters u, v, w, $\Delta\phi_\mathrm{x}$, $\Delta\phi_z$ and h to describe a paraboloid as proposed by VON HOERNER [Hoe67a] (see figure 4.10). A paraboloid parametrized with this six variables provides direct access to translation and rotation movements in the 3–dimensional space as well as a change in the focal length. As mentioned in section 2.3.2, the u, v and w describe a translation of the vertex. The angles $\Delta\phi_\mathrm{x}$ and $\Delta\phi_\mathrm{z}$ indicate a rotation around the x- or the z-axis. h is a parameter for the focal length - consequently a measurement for the curvature of the paraboloid.

A paraboloid in three–dimensional space could be described by

$$y = ax^2 + az^2 \tag{4.13}$$

whereat $a = \frac{1}{4f}$.

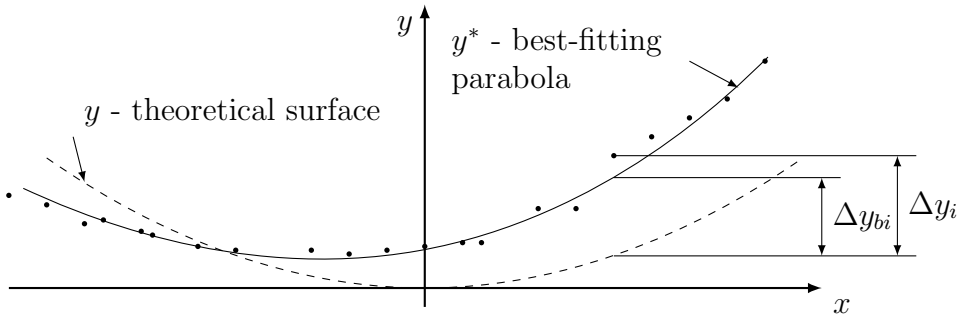

Figure 4.9: Theoretical surface, computed position of nodes for the deformed surface and the best-fitting parabola (2-dimensional)

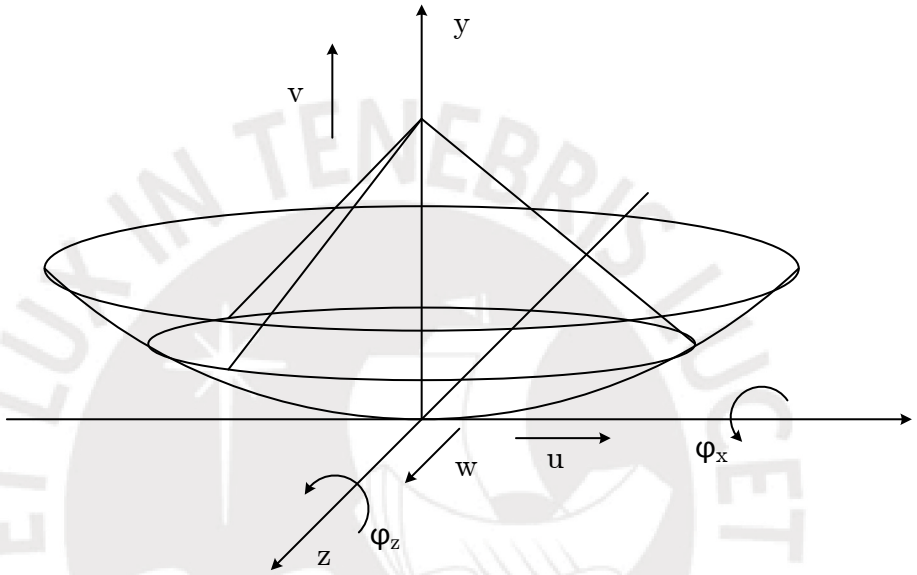

Figure 4.10: Coordinate system on the paraboloidal reflector surface

Translation

A translational displacement (u,v,w) of this paraboloid results in an offset as follows

$$y^* = a\,(x-u)^2 + a\,(z-w)^2 + v \tag{4.14}$$
$$= ax^2 - 2aux + au^2 + az^2 - 2awz + aw^2 + v \tag{4.15}$$

With equation (4.13) it is possible to declare one term as the original untranslated paraboloid y and write

$$y^* = y - 2aux + au^2 - 2awz + aw^2 + v \tag{4.16}$$
$$\Delta y = -2aux + au^2 - 2awz + aw^2 + v \tag{4.17}$$

Because of the expected small translational displacement, it is possible to neglect the quadratic terms au^2 and aw^2 to simplify to

$$\Delta y = -2aux - 2awz + v \tag{4.18}$$
$$= -2\frac{1}{4f}ux - 2\frac{1}{4f}wz + v \tag{4.19}$$
$$= -\frac{x}{2f}u - \frac{z}{2f}w + v \tag{4.20}$$

Rotation

The angles ϕ_x and ϕ_z respect a rotation of the paraboloid around the x- and z-axis. For small angles the y-displacement due to a rotation could be described as

$$\Delta y = -x\phi_z + z\phi_\mathrm{x} \tag{4.21}$$

Change of the focal length

The parameter h describes the bend of the paraboloid thus it is a quantity for the focal length. According to [Kat70] a change in y–direction due to an alteration of the focal length results in

$$\Delta y = \frac{x^2 + z^2}{4}\left(\frac{1}{f^*} - \frac{1}{f}\right) \tag{4.22}$$
$$= \frac{x^2 + z^2}{4f}\left(\frac{f}{f^*} - 1\right) \tag{4.23}$$
$$= y\left(\frac{f}{f^*} - 1\right) \tag{4.24}$$

Superposition of all transformations

For an arbitrary paraboloid following the equation of (4.13) shifted and rotated in space with a changed focal length follows

$$y^* = y - \frac{x}{2f}u + v - \frac{z}{2f}w + z\phi_\mathrm{x} - x\phi_z + y\left(\frac{f}{f^*} - 1\right) \tag{4.25}$$

With $h = \left(\frac{f}{f_n} - 1\right)$, it is possible to express it with 6 parameters and prepare it to compose a linear equation system:

$$y^* = y - \frac{x}{2f}u + v - \frac{z}{2f}w + z\phi_\mathrm{x} - x\phi_z + yh \tag{4.26}$$

Equation (4.26) delivers a solution to express the new paraboloid y^* via the theoretical surface y and 6 fitting parameters whichever could translate, rotate and inflect it. To

determine these unknowns for the actual plane, the linear system of equations $\boldsymbol{Ap} = \boldsymbol{b}$ (4.27)(similar to [WD07]) has to be solved.

$$\begin{pmatrix} -\frac{x_1}{2f} & 1 & -\frac{z_1}{2f} & z_1 & -x_1 & y_1 \\ \vdots & \vdots & \vdots & \vdots & \vdots & \vdots \\ -\frac{x_n}{2f} & 1 & -\frac{z_n}{2f} & z_n & -x_n & y_n \end{pmatrix} \begin{pmatrix} u \\ v \\ w \\ \phi_{\mathrm{x}} \\ \phi_z \\ h \end{pmatrix} = \begin{pmatrix} y_1^* - y_1 \\ \vdots \\ y_n^* - y_n \end{pmatrix} \tag{4.27}$$

The parameter vector $\boldsymbol{p}$ represents the geometrical variables directly – with the exception of the parameter h. The essential information out of h is the change of the focal length $\Delta f = f^* - f$. The equation 4.24 offers Δf via

$$\begin{aligned} h &= \frac{f}{f^*} - 1 \\ f^* h &= f - f^* \\ f^*(h+1) &= f \\ f^* &= \frac{f}{h+1} \end{aligned} \tag{4.28}$$

With this expression the change of the focal length is

$$\Delta f = \frac{f}{h+1} - f \tag{4.29}$$

4.2.1 Solution for the best-fit optimization problem

Computational approach

The best-fitting paraboloid is defined by the parameter vector $\boldsymbol{p}$. This can be delivered by the solution of the equations (4.27). An equation system is uniquely solvable if the rank of the matrix $\mathrm{rank}(\boldsymbol{A}) = m$ equals the rank of the extended matrix $(\boldsymbol{A} \mid \boldsymbol{p})$. For the case of the linear system of equations (4.27) it is assumable that there is no such unique solution for the parameter vector x. One row represents an equation for a surface point. Normally the system (4.27) has to deal with significantly more than 6 rows such as shown in figure 4.8 with 282 surface points. If there are more equations than unknown variables this system is called overdetermined. This seems to be a possible case because of the large number of surface points. Such a situation induces a problem of the adjustment theory.[BHL+08]

While this is a comprehensible case another possibility should not let be disregarded. The numerical solution is restricted to the floating-point precision of the calculating program (in this case MATLAB). A problem may occur while the matrix $\boldsymbol{A}$ consists of numerous rows with coordinate values close to each other. Even the matrix holds exclusively linearly independent columns, due to the finite-precision it appears to be singular. Hence the computation assumes to deal with an underdetermined system

because of its deficient rank. [Cle04]

Following [Cle04] MATLAB offers an operator to compute the solution to

$$\boldsymbol{A}\boldsymbol{p} = \boldsymbol{b} \tag{4.30}$$

for an arbitrary equation system. This function is called backslash-operator and solves the problem automatically in a least-squares sense.[Mat14] The algorithm solves the system predominantly using the QR-factorization - an orthogonalization algorithm. As expected, the test cases for the actual problem delivered a system with deficient rank rank($\boldsymbol{A}$) = 4. But [Cle04] claims that the solution obtained from the backslash–operator in degenerated situations does not guarantee uniqueness. [BHL$^+$08][Cle04]

Many of the publications like [CYX13] or [WDQ$^+$04] do not solve the equation system directly but using the normal form. This method uses the Gauss–Transformation to transform it into six equations with six unknowns as the system matrix will be square. The method uses the least square approach from [BHL$^+$08]

$$r_i = \sum_{k=1}^{n} a_{ik} p_k - b_i \tag{4.31}$$

with the residuals r_i. Forcing the quadratic sum of the residuals to be minimal leads to the rms from equation (2.9) Nevertheless this also faces the problem concerning the deficient rank. Because then the square matrix $\boldsymbol{A}^T\boldsymbol{A}$ is singular and the inverse $\left(\boldsymbol{A}^T\boldsymbol{A}\right)$ is not defined. This causes the normal equations

$$\boldsymbol{p} = \left(\boldsymbol{A}^T\boldsymbol{A}\right)^{-1}\boldsymbol{A}^T\boldsymbol{b} \tag{4.32}$$

to collapse. An alternative to the inverse of a matrix is the so called pseudoinverse. This is sometimes referred to as the generalized inverse. In case of MATLAB the function pinv() will use the Moore–Penrose version of a pseudoinverse matrix. [BHL$^+$08][Cle04]

Another solution offers the MATLAB curve fitting toolbox *cftool* (older versions of MATLAB come with the surface fitting tool *sftool*). This program provides a graphical user interface for solving nonlinear curve fitting tasks.[Cle04] With it's help it is possible to find the parameters for a custom function like the fitting–paraboloid from equation (4.26). The tool is instructed to run an optimization with the Levenberg–Marquardt algorithm (LMA). This is a least-squares fitting using the Gauss–Newton procedure. [Lou05]

For the solution of the equations (4.27) to find an accurate description of the reflector surface three methods were used:

- MATLAB backslash operator
- solution of the normalized equation system

- MATLAB curve fitting toolbox *cftool*

Comparison of the results

To compare those results the root–mean–square error from equation (2.9) for every fit in different elevation angles was calculated and is shown in table 4.3. In the literature this is a common proof of the accuracy of a curve fitting. The accuracy of the backslash-solver and the normal equations are almost similar. The difference is small and not visible with the displayed precision. Hence the fitting results from these two methods are assumed to be very close to another. The *cftool* calculates a fitting curve with a residual rms error 10 times higher. All methods are getting better fitting results for the load situations with higher elevation angles (compare the full look-up tables in the appendix 6). This may be caused by a less deformed reflector surface for the upright position. Fewer deformation means a lower departure from the ideal paraboloidal shape and therewith a better fitting result to the function of a paraboloid.

Table 4.3: Comparison of the solving methods using the RMS error

	10 °	55 °	90 °
backslash-solver	$2.0496 \cdot 10^{-5}$mm	$1.5886 \cdot 10^{-5}$mm	$1.0064 \cdot 10^{-5}$mm
normal equations	$2.0496 \cdot 10^{-5}$mm	$1.5886 \cdot 10^{-5}$mm	$1.0064 \cdot 10^{-5}$mm
cftool	$3.4791 \cdot 10^{-4}$mm	$2.6965 \cdot 10^{-4}$mm	$1.7084 \cdot 10^{-4}$mm

4.2.2 Interpretation of the numerical solution

The simulation in ANSYS was performed for different elevation angles from 10 ° up to 90 ° in steps of 5 °. Each load situation delivers its own point cloud of surface nodes and therewith an individual equation system (4.27). The three mentioned methods to solve are applied to each simulation result. The full results of the computed fitting parameters are collected in three look-up tables in the appendix 6. These tables will be the basis of the focal point correction. Such tables are a common tool to correct known and repeatable errors like the dead weight deformations.[Gaw04] Table 4.4 shows an excerpt of the solved normal equations for three elevation angles. The change of the focal length D_f is calculated separately from parameter h using equation (4.29).

Table 4.4 presents an impression of the magnitude of the parameters. The translational shift of the vertex point is dominated by v in the y-direction. The shift in x is small in comparison to this and there is almost no impact in z-direction. For the two rotations the fitting angle ϕ_x is small and negligible compared to ϕ_z. The rotation around the z-axis and the translational shift u appears small in comparison to their related movements. But in combination both superimpose each other to a movement in x–direction. Therefore as significant fitting parameters u, v, the angle ϕ_z and the change of the focal length D_f are chosen. The shift w as well as its corresponding tilt

Table 4.4: Solution from the normal equations for selected elevation angles (în addition with the change of the focal length D_f)

ψ	u	v	w	ϕ_x	ϕ_z	h	D_f
°	mm	mm	mm	°	°	1	mm
10	0.01401	−0.48992	−0.00013	0.00011	0.01166	−0.00607	44.31951
55	0.00828	−0.42028	0.00003	−0.00003	0.00689	−0.00598	43.70657
90	0.00017	−0.40156	0.00015	−0.00012	0.00014	−0.00596	43.53416

angle ϕ_x will be neglected.

Figure 4.11 shows the focal length as a function of the elevation angle. The original focal length of 7.26 m is not shown in this diagram. The actual distance outreaches the intended one in every elevation of the telescope with around 44 mm. For an increasing inclination the focal distance reduces in a non-linear behaviour. The covered range is small with a value around 1 mm.

Figure 4.12 shows the x–y–plane of two examples for best fitting paraboloids. Any displacement in the z–direction is neglected due to its small influence. To compare them with the designed shape of the reflector, the theoretical surface is plotted as well. The curves are calculated using the fitting equation (4.26) with the parameter vector

$$\boldsymbol{p} = \begin{pmatrix} u & v & w & \phi_\mathrm{x} & \phi_\mathrm{z} & h \end{pmatrix}^T \tag{4.33}$$

for the elevation angles 10 ° and 90 °. The theoretical surface is plotted following the RT–20–paraboloid from equation (4.12) over the complete diameter 20 m. The displayed curves experienced a transformation simultaneously over the six parameters. Therefore a proper discussion is difficult. But there is an obvious shift in the axial direction for the actual surface functions. The vertex region of the telescope settles down in comparison to the theoretical surface. But it lifts slightly while tilting up to the face–up position. Furthermore a small offset in x–direction is recognizable.

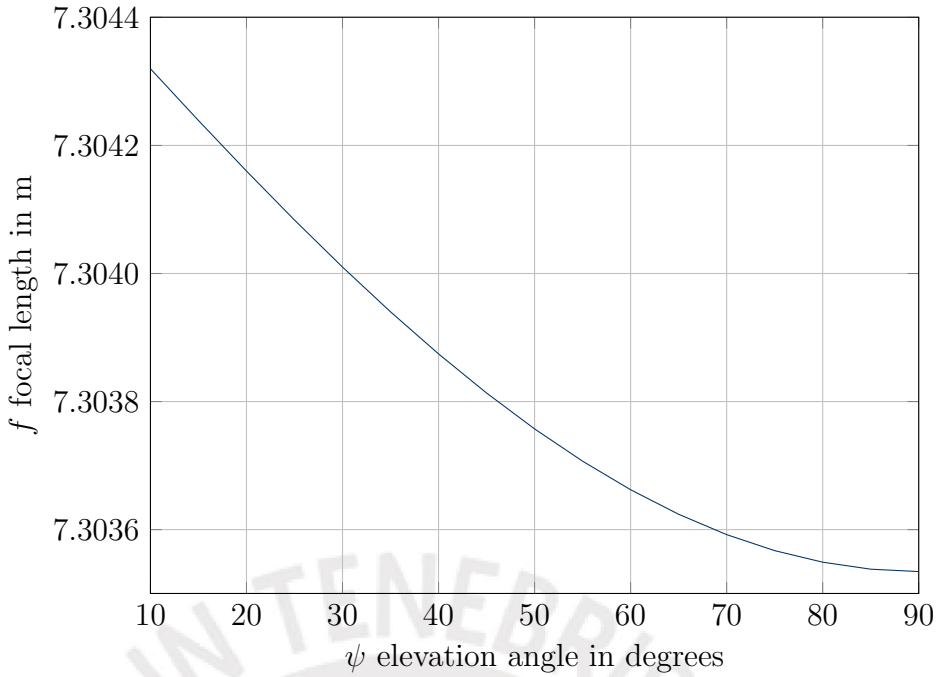

Figure 4.11: Focal length of the INRAS RT-20 as a function of the elevation angle

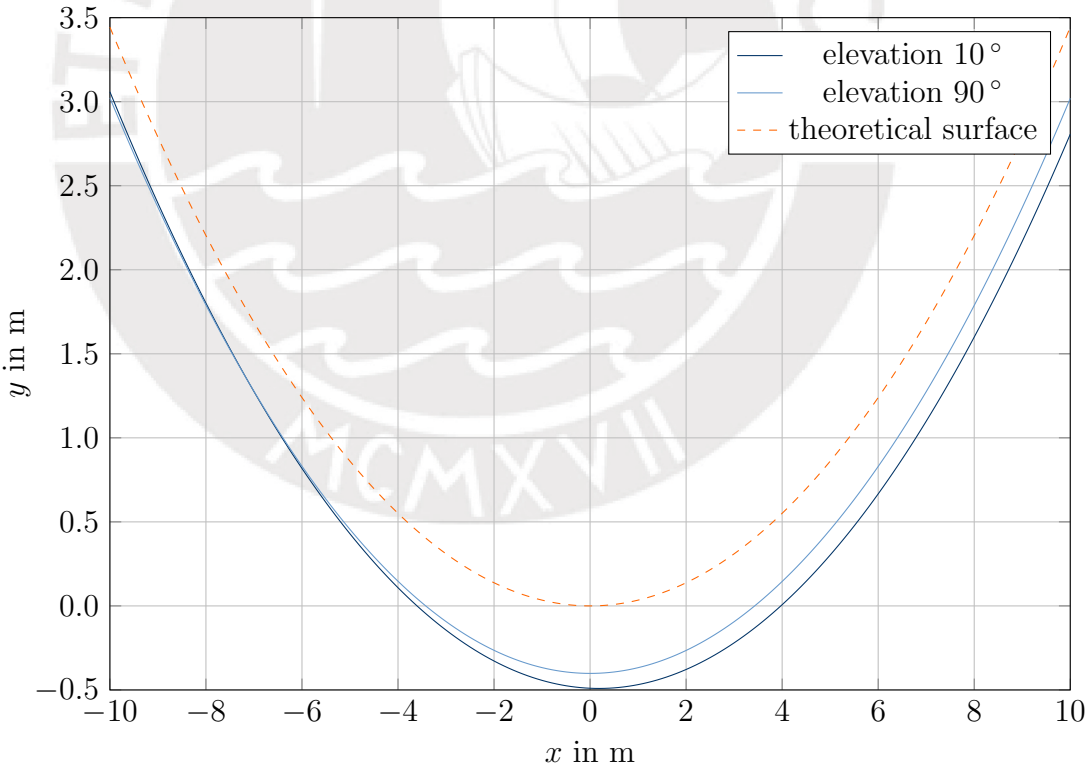

Figure 4.12: Cross section in x-y-plane best-fit paraboloids at the elevation angles 10 ° and 90 ° in comparison to the theoretical surface

4.3 Determination of the focal shift

The derivation of the best fitting paraboloid from section 4.2 provides the parameters of the new paraboloidal reflector surface. With this information it should be possible to calculate the position of the new focal point. This should coincident with the location of the aperture plane of the primary antenna, the feed horn, to use the maximum performance of the telescope. As this is not incidentally the case, the position of the feed horn has to be adjusted by a suitable actuation system (see chapter 4.5).

The quantity to minimize by the actuation system is the offset between the feed horn aperture and the focal point. Both locations are changing simultaneously. So it is necessary to observe the geometry of the paraboloid as well as the position of the feed horn. Furthermore the movements are correlated because the primary antenna upon the tripod is mounted on the backing structure of the reflector. The tripod stand passes the bending and deformations of the support structure to the feed. The simulation in ANSYS is fed with the information about the tripod structure and its properties. So this movement is easy to determine using the results of the simulation.

It should be appropriate to use the absolute coordinates from the numerical solution in ANSYS. It delivers the actual feed position and the parameters to determine the location of the focal point out of the deformed reflector paraboloid. The vector between these two points is the needed correction movement of the feed horn.

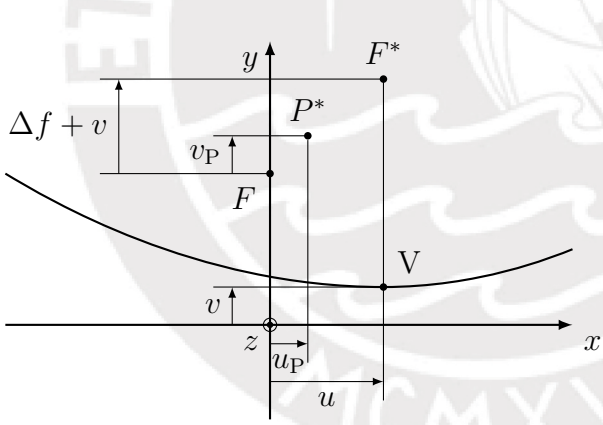

(a) Focal shift due to the translational displacement with P as the reference point located on the feed horn

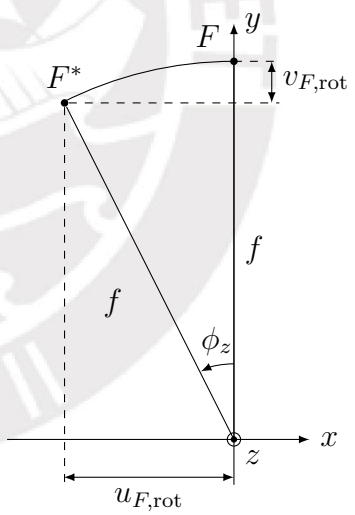

(b) Focal shift due to angle ϕ_z

Figure 4.13: Parameters to describe the focal shift

It is common to distinguish the axial from the lateral defocus like in [Baa07] and reduce the misalignment of the feed and the reflector surface to these two parts. Looking at the relevant fitting parameters discussed in section 4.2.2 this should be an appropriate

approach for the actual work as well. The best-fit-paraboloid can be described adequate using the four parameters u, v, ϕ_z and h (respectively D_f). Figure 4.13 illustrates all these qualities and their impact to the relative movement between feed horn and the reflector surface. The figure 4.13a shows the misalignment due to a rotation of the reflector paraboloid with angle ϕ_z. The caused shifts along the x- and z-axes are covered by the examination of the axial together with the lateral defocus. The tilt caused by the angle ϕ_z will be neglected because of the small impact and has only a small effect to the antenna gain. This assumptions implicate that the body fixed coordinate system of the feed horn has only axes parallel to (x, y, z).

4.3.1 Axial defocus

The axial defocus denominates the displacement of the focal point parallel to the vertical axis y. The position of the focus in the coordinate system (x, y, z) is determined by the position of the paraboloid and its geometry. The curve fitting yields to a paraboloid with a vertex shifted by the offset v. Consequently its focal point must experience the same displacement.

Another factor arises from the change in the curvature of the theoretical and the best-fitting surface. Following the theory of the homologous design the curve remains as a paraboloid of revolution. Thus it retains with its one focal point and the displacement continues along the axis of symmetry. Presumably only the focal distance changes as Δf depending on the new curvature.

If the best-fit paraboloid is not only translated in space but also rotated, the gyration ϕ_z contributes to the displacement of the focus. To be seen in figure 4.13a the dislocation in axial direction can be described by

$$\begin{aligned} v_{F,\mathrm{rot}} &= f - f\cos\phi_z \\ &= f(1-\cos\phi_z) \end{aligned} \tag{4.34}$$

These parameters altogether deliver the equation for the displacement of the antenna's focal point in axial direction in reference to (x, y, z):

$$\begin{aligned} v_F &= v + \Delta f - v_{F,\mathrm{rot}} \\ &= v + \Delta f - f(1-\cos\phi_z) \end{aligned} \tag{4.35}$$

Consequently the relative movement between the reflector surface and the feed horn in this direction is

$$\begin{aligned} y_{off} &= v_F - v_P \\ &= v + \Delta f - f(1-\cos\phi_z) - v_P \end{aligned} \tag{4.36}$$

with v_P as the axial displacement of the reference point P on the feed horn.

4.3.2 Lateral defocus

The derivation of the lateral defocus follows the same pattern. Figure 4.13 shows the distances show the distances of the displacement in x–direction. Following the former convention the translation of the vertex is denominated by u. As well as for the axial displacement the rotation around ϕ_z (see figure 4.13a) contributes

$$u_{\mathrm{F,rot}} = f \sin \phi_\mathrm{z} \tag{4.37}$$

to the offset. Both influences sum up to the shift of the focal point

$$\begin{aligned} u_\mathrm{F} &= u - u_{F,\mathrm{rot}} \\ &= u - f \sin \phi_\mathrm{z} \end{aligned} \tag{4.38}$$

Hence the relative movement between the antenna's focal point and the feed horn is

$$\begin{aligned} x_\mathrm{off} &= u_\mathrm{F} - u_\mathrm{P} \\ &= u - u_{F,\mathrm{rot}} - u_\mathrm{P} \end{aligned} \tag{4.39}$$

The two equations (4.36) and (4.39) provide the information about the offset between the feed position and the actual focal point. Hence they compose the vector for the correction movement to apply to the antenna feed so that

$$\begin{pmatrix} x_\mathrm{off} \\ y_\mathrm{off} \end{pmatrix} = \begin{pmatrix} u - u_{F,\mathrm{rot}} - u_\mathrm{P} \\ v + \Delta f - f(1 - \cos \phi_\mathrm{z}) - v_\mathrm{P} \end{pmatrix} \tag{4.40}$$

Table 4.5: Calculated focal offset for a selection of elevation angles (based on results from the normal equations)

ψ °	x_off mm	y_off mm
10	−3.87395	43.33803
55	−2.46442	42.62472
90	−0.28980	42.60990

4.4 Implementation in a program sequence

The former discussed methods and algorithms are implemented in scripts for ANSYS APDL and MatLab. Figure 4.14 shows the intended workflow and links between the scripts. The simulation scripts require the input geometry of the telescope as a line model provided by Model.igs. The scripts are equipped with the information derived in the present chapter and are executed one after another. 3_solution.txt iterates

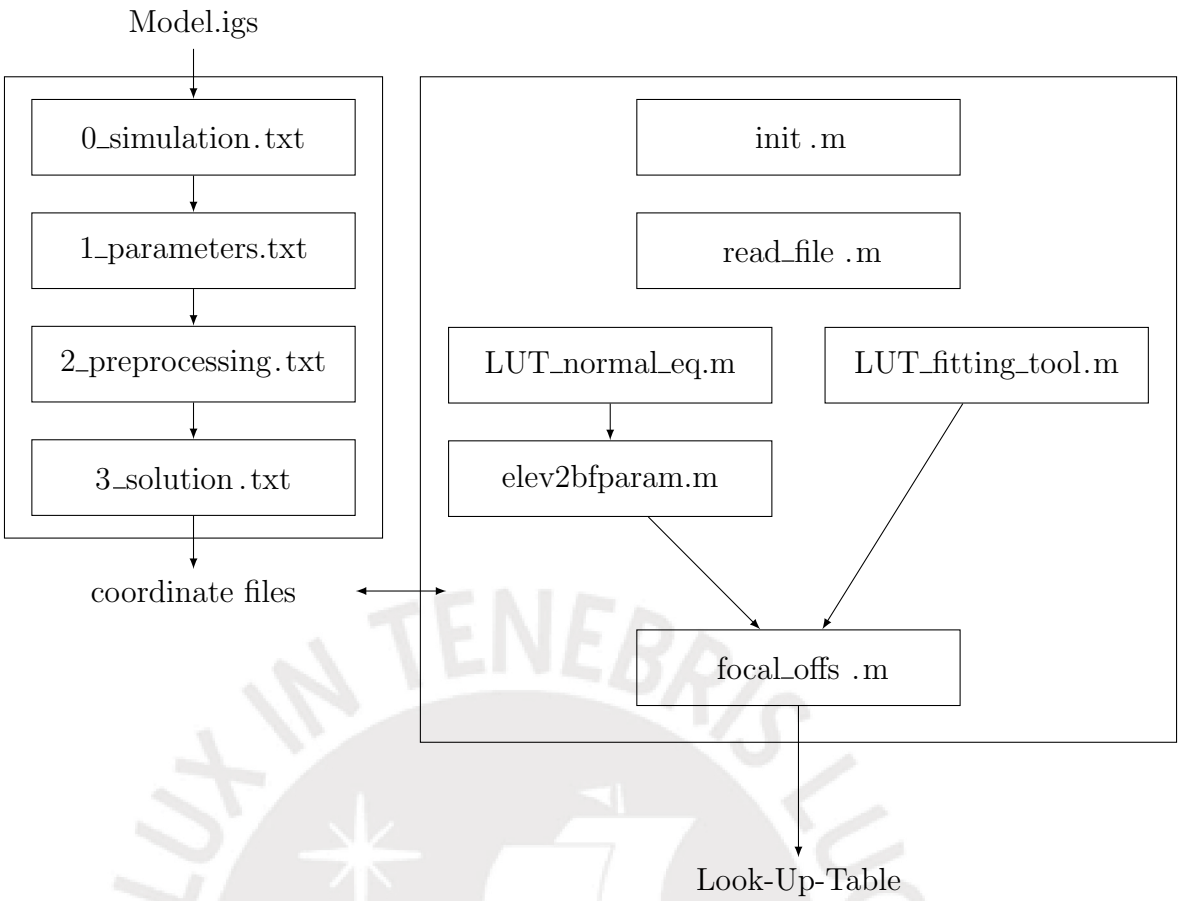

Figure 4.14: Simulation in ANSYS (left) and BFP-algorithm in MatLab in a program sequence

through the load cases with changing elevation angle while printing the results in coordinate files.

The MatLab-part is divided in two sequences depending on the preferred solving tool. Either the solution via the normal equations (with an option for the backslash operator) or the cftool can be chosen. Both use the routines of init .m for the initialization and read_file .m to read the coordinate files from the ANSYS-output. To calculate the focal shift the script focal_offs .m is called. Independent of the selected solver, a Look-Up table like in chapter 6 is generated.

4.5 Systematic errors of the simulation

The shown approach is based on various assumptions. Some of them arise from unknown properties of the radio telescope in its design phase. Others are caused by modelling a complex real situation in a simulation software, the numerical solution

and simplifications.

The model of the reflector backing structure is built by meshing the geometry of the frame work with the cross sections of the bars. The lines of the model are crossing each other in nodes and consequently the meshed cross sections cover the whole length of a line. In the model the frame work beams overlap each other in the environment of these nodes. This is not an adequate description of the reality because physics would not allow such a merge of bodies. While the deformation would be simulated properly there is an additional mass which does not exist in reality. This influences the effect of the dead weight deformation of the telescope.

For the simulation the cross sections are meshed with the line model without considering the changing orientation of the frame work bars. The meshing algorithm installs every section with its axes parallel to the global coordinate system. Hence all beams have the same orientation. In reality the orientation of a beam depends on its position on the reflector structure. With increasing distance from the center the beams keep an orientation normal to the paraboloidal shape. This tilting is not modelled.

A more obvious discrepancy occurs due to the absence of the reflector surface. This issue was examined in section 4.1.1 and considered to have a small impact on the further calculations. This regards only to the geometry. Another aberration appears from the lack of mass. In comparison to the backing structure the mass of the aluminium panels is assumed to be small and was not included in the simulation. This decision is also based on examination of other publications like the simulation shown in [WD07] or [Gaw04].

CHAPTER 5

Mechatronical design of an actuator for the adjustment of the primary antenna

5.1 Specification and requirements

The INRAS RT-20 will not be equipped with an active surface mentioned in section 2.1.1. So the readjustment of the defocussed telescope has to fall back on a compensatory movement between the primary antenna and the reflector surface. Although it appears to be possible to align the reflector backing structure, usually this is not the preferred solution. Due to its weight and the telescope setup, this is not a suitable method. Rather than this, the primary antenna is destined to be movable. The required actuator is designated to be the centerpiece between the tripod structure and the primary antenna. The main function is the fixation of the feed horn on the head of the three tripod legs. In addition an actuation system implements the possibility to adjust the feed relative to the reflector surface. This alignment is designated to assure the coincidence of the aperture-plane centre of the primary antenna and the focal point of the reflector.

To offer a reproducible and well justifiable solution the design process of the actuator will be orientated in parts on the methods of the VDI2221 [VDI93] and VDI2206 [VDI04]. At the beginning a full list of requirements will be erected. Based on this table, a variety of suitable technical concepts will be developed. Thereon an assessment by means of selected criteria is performed. Out of this analysis a favoured design emanates as the most suitable concept. At the end of the actual work a recommendation for an actuation system will be given.

A full list of requirements is shown in table 5.1. The following sections will discuss the issues in a more detailed explaining the background of the requisitions.

5.1.1 Functional requirements

The required degree of freedom was already discussed in sections 4.2.2 and 4.3. Since the remaining correction movements are reduced to axial and lateral alignment the required degree of freedom of the actuation system is two. One translation in x and the other along the vertical axis y. But when handling the mount of the primary antenna requirements from other fields arise as well. From the electromechanical view it can be useful to adjust the feed polarisation. So a rotation around the vertical axis with angle ϕ_y is desirable. Bringing this together with the correction of the homologous deformation yields to a degree of freedom equal 3.

The main task of the actuator will be the one-dimensional translational in y movement of the antenna mount against its counterpart on the tripod to meet the changed focal length. This movement has to cover the distance to adjust the feed horn in axial direction. Hence in minimum the calculated offset y_{off} from section 4.3.1. For this motion a covered distance of 45 mm is sufficient. But in operation it can be useful to be able to adjust the feed horn in the dimension of a wave length. Hence the requirement will be amplified until covering half the period of the maximum wavelength $\lambda_{\max}$ to be observed. This arises from the projected frequency range of the telescope with $1.42\,\text{GHz} \leq f \leq 15\,\text{GHz}$. As the wavelength λ depends on the frequency f like

$$c = f\lambda \tag{5.1}$$

the corresponding wavelength could be obtained. The minimum frequency $f_{\min} = 1.42\,\text{GHz}$ delivers the longest wavelength

$$\lambda_{\max} = \frac{c}{f_{\min}} \approx 211.12\,\text{mm}. \tag{5.2}$$

According to the needs of the INRAS institute $0.5\lambda_{\max}$ is the minimum distance to be covered by the actuator. To work with a common value and provide a buffer the distance will be set to $y_{\text{P}} = 110\,\text{mm}$.

The lateral defocus is small in comparison the axial one. Following table 4.5 a compensating movement of approximately 5 mm is enough. To add some additional freedom for adjusting movements for instance the range will be stretched to $x_{\text{P}} = 20\,\text{mm}$.

The precision of the adjustment also corresponds to the wavelength. The desired resolution of the radio telescope is $0,1\lambda_{\min}$. With

$$\lambda_{\min} = \frac{c}{f_{\max}} \approx 19.98\,\text{mm} \tag{5.3}$$

the minimum precision to be reached will be set to $0,1\lambda_{\min} \approx 1\,\text{mm}$.

The velocity is not a critical fact as the claimed movement range is. The velocity of the actuator corresponds to that of the reflector. It has to reach its calculated position in the same time like the reflector elevates or rotates to always provide a proper focussed telescope. The rotation in azimuth does not concern the feed adjustment. Solely the elevation movement sets requirements to the actuation system. The velocity during operation is expected to be small. While pointing to a radio source in the sky only the rotation of the earth need to be compensated. For this reason it is assumed that the duration for an arbitrary adjustment motion is much more decisive. To not restrain any other measurement the maximum duration for an adjustment it set to 10 s.

The biggest feed horn has a mass of around 13 kg. This is the maximum mass to move but an important design parameter. The actuator has to hold and move the feed under changing direction of the gravity. This is an essential requirement, because of the wide range of elevation angles of the telescope.

5.1.2 Weather and climate conditions

The actuation system has to be designed as an outdoor-device. It will be exposed to all weather conditions by itself yielding to special and challenging exigencies of the design. The actuator's whole lifespan it will be mounted to the antenna feed of the telescope.

The intended working site is Lima, Peru. In the classification of Köppen and Geiger the climate of this region is classified as *BWk*. This abbreviation denotes an arid desert environment with little rainfall. *k* stands for an average annual temperature below 18 °C. The highest average temperature of the year of 22.3 °C is reached in February and the lowest in August with 15.1 °ircC. Hence the variations in temperature over the year are small. The rainfall reaches its maximum in august with 7 mm while staying the half of the year close to zero.[Hey72]

5.1.3 Technical environment and interfaces

Every feed horn has basically a cylindrical shape with a circular section. The lower part is dominated by a bearing-out. The imaginary plane located at the lower edge of this disc composes the aperture plane. The focal point is situated at the intersection of this plane with the symmetry axis of the cylinder. This is the focal point of the primary antenna which ought to coincident with focus of the reflector.

The INRAS radio telescope is designed to deal with various frequencies. As mentioned in section 2.1.1 the reflector suits a wide band of frequencies. But a feed horn is dedicated to a special wavelength. Hence the primary antenna must be interchangeable

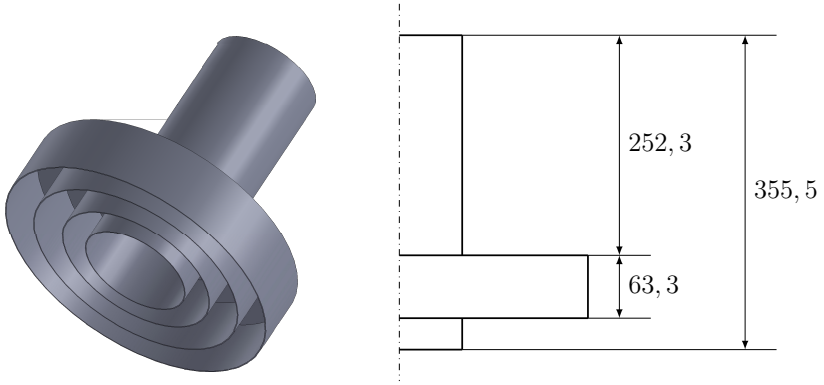

(a) Model in SolidWorks (b) Dimensions

Figure 5.1: The feed horn of the RT-20 for a frequency of 1420 MHz

to work with more than one frequency. The radio telescope of the INRAS is working with feed horns with diameters between 47.4 mm and 355.5 mm amongst others. Figure 5.1b show the dimensions of the 1420 MHz-feed. To deal with several diameters a mechanical adapter will be necessary to provide a suitable mount for every feed horn. This mechanical adapter could be attached to the feed horn permanently. The interface between adapter and actuation system then is standardized to provide easy exchangeability.

The feed horn has a thin walled section. This sets important restrictions to the connection method. Boring into the thin wall is applicable because of the stability. Furthermore additional shadowing of the radiation caused by any form fitting part is not justifiable. A feasible method to combine adapter and feed horn is a material connection like welding.

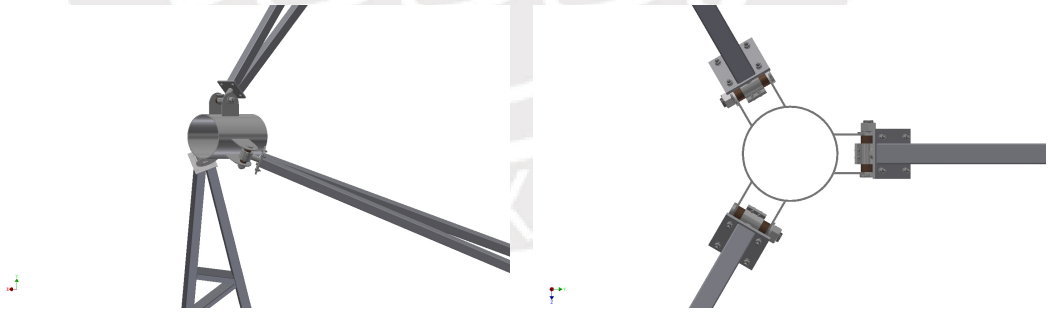

(a) isometric view (b) from below

Figure 5.2: Tripod head and bearing of a feed-dummy

The radio telescope will provide electrical energy with 48 V direct voltage. This could be used to drive electric actuators. The power supply is needed at the head of the tripod as well as any kind of control signal. While there are other cables and supplies this is only an additional wiring from the ground up to this point. In the actual design

they are guided through one or more tripod legs.

Figure 5.2 shows a model of the tripod-head. The three tripod legs meet each other in this points holding a tube as a dummy for the primary antenna respectively the actuation system. Every leg is pivoted at its lower end. So each can pan around this mounting point. This allows to mount components with different diameters at the tripod-head and provides a variable space for any extension at the top.

5.1.4 Table of requirements

Nr.	Function	Value	comment
Functional requirements			
F01	automatic positioning	-	
F02	self locking	-	no need of power to hold idle state
F03	interchangeable adapter	-	to install different feed horns
F04	reaction to perturbation	emergency stop	
F05	position sensing	absolute	for translation and rotation
M06	translational DOF	2	along x-axis and y-axis
M07	rotational DOF	1	around vertical axis with angle ϕ_z
M08	translation along y-axis	$y_\mathrm{P} \geq 110mm$	
M09	translation along x-axis	$x_\mathrm{P} \geq 20mm$	
M10	angle of revolution around y-axis	$\geq 180°$	
M11	positioning duration for rotation	$\leq 5\,\mathrm{s}$	to reach any angle $0 \geq \alpha \geq 180°$
M12	positioning duration for translation	$\leq 10\,\mathrm{s}$	to cover the whole movement range
M13	precision translation	$\pm 1mm$	
M14	precision rotation	$1°$	
M15	minimum mass to move	$13\,\mathrm{kg}$	weight of the feed horn
Structure			
F16	material	resistant to deformation, weatherproof, lends itself to machining	
F17	mount of antenna feed	no change on geometry of the feed horn	no drill hole, no forming
F18	interchangeability of the feed horn	universal interface	adapter piece
F19	mount on tripod structure	-	

M20	dimensions	preferably small	low additional shadowing on the reflector
M21	maximum empty weight	17 kg	weight of the actuation system
W22	use of given structure	-	no changes on the rest of the antenna structure
Environment and interfaces			
F23	energy supply	48 V DC	
F24	site of operation	outdoor	Lima, Peru
F25	insensitive to electromagnetic influences	-	
M26	assure protection class	IP54	insensitive to pollution and rain (DIN EN 60529:2000)
M27	average annual temperatur	$\approx 15 - 23°C$	
M28	insensitive to direct sunlight		heating of exposed components
M29	humidity range	0% - 90%	[1]
Maintenance and Use			
M30	operation time	$12^h/_{day}$	
M31	endurance	5 years	
M32	disposability	$\geq 90\%$	
W33	cost of operation	$\leq$ 200 PEN per month	
W34	maintainability	through service personnel on-site	
Production			
F35	Number of pieces	1	unique specimen
W36	Actuators, control, sensor system	standard parts	
W37	Avoiding of special parts	-	simple fabrication
Safety			
F38	user interface	emergency switch	

Table 5.1 shows a list of the requirements, collocated in the sections before. This provides the orientation for the design process of the actuation system. Entries marked with F are fixed claims without any tolerance in fulfilment. Requirements marked with M have to be satisfied in minimum to their lower limit. Every W-entry is desired but abdicable.

[1] http://www.temperatureweather.com/pacific/wetter/de-wetter-in-peru-lima.htm, 04.05.2015

5.2 Comparison of actuation principles

5.2.1 Serial Actuation

A first guess to realize the required motions is to use one actor for each movement. A sequence of actuated one-degree-of-freedom links builds a serial actuation system. Such a set-up needs two translational actuators and one rotational one, thus three generalized coordinates. Each of them may be equipped with an additional gearing mechanism and corresponding suspensions. This allows separated movements for each generalized coordinate.

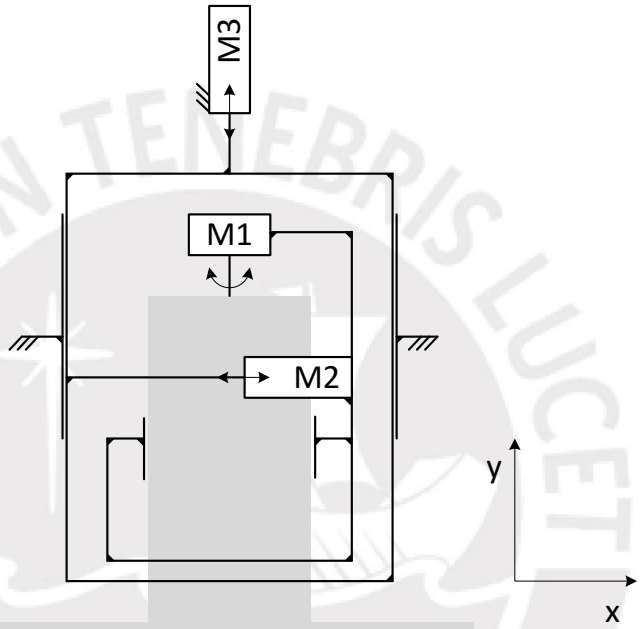

Figure 5.3: Principle of the serial actuation

The principle is shown in figure 5.3. The order of the actuation is variable and customizable. The figure shows a feasible sequence. The rotatory motion around the vertical axis is realized as the innermost movement and geared by motor M1. The rest of the actuation system is arranged as a rack driven by the two linear actuators M2 and M3. Corresponding bearings for each motion have to assure a reliable guidance and track. Actuator M3 moves the entire frame and is linked to the base itself.

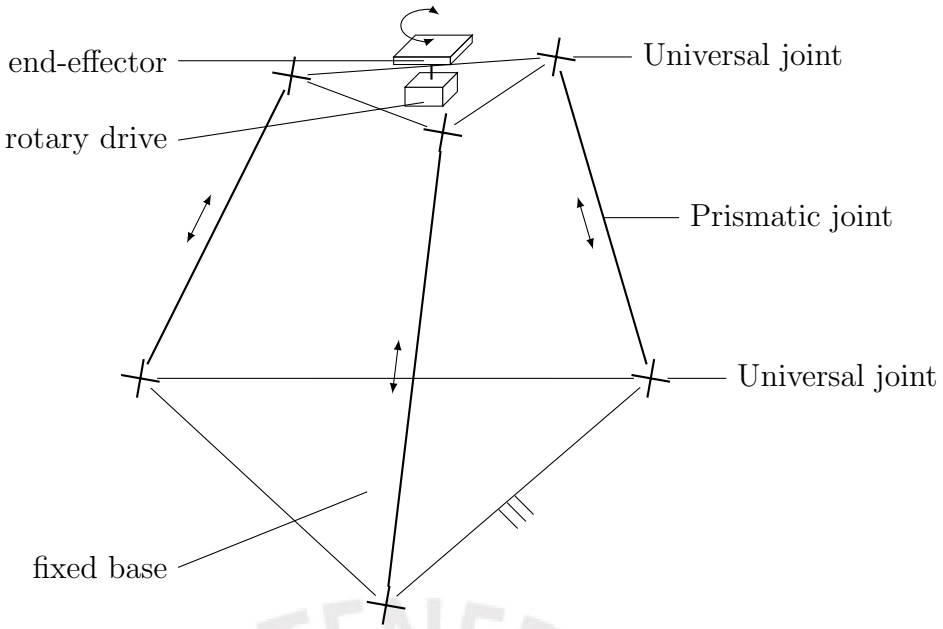

Figure 5.4: Delta mechanism in UPU configuration from [JT03] extended by an additional rotary drive

5.2.2 Integrated delta mechanism with linear actors in the tripod legs

A more elegant way than the serial actuation is making use of parallel-kinematic mechanisms. Jean-Pierre Merlet presents in [Mer06] a wide diversity of parallel mechanisms for a degree of freedom from one up to six. A parallel manipulator often consists of several limbs connecting a movable platform with a fixed base. It is in common to use one actuator to drive one leg. And thereby working with a degree of freedom equal to the number of actuators. The actuators can be placed close to the fixed base. This results in a low mass inertia of the moved parts of the architecture. This allows in particular high speed applications which are not needed for the actual problem yet. A big advantage of parallel mechanisms arises from the closed loop kinematic chain. They offer an exceeding good stiffness and in general a high precision movement. [JT03][Mer06]

For the actual case two translational movements and a rotation around the vertical axis are needed. [JT03] discusses a 3-DOF mechanism with exclusively translational movements. A variation of this, with an additional rotary drive is shown in figure 5.4. This principle consists of three actuated legs supporting a movable platform. All three limbs consist of an equal kinematic structure. It is also called 3-UPU parallel manipulator because of its architecture. Each leg with an actuated prismatic joint P is linked to the fixed base as well as to the moving platform with a universal joint U. A limb has a degree of freedom equal to five. This assures one constraint to the moving platform. [JT03] refers to the publication [TJ00] which shows that the arrangement can restrict all rotatory motions of the platform. So pure translational movements remain.

Following [Mer06] the equation of Grübler for three-dimensional problems delivers the degree of freedom F with

$$\mathrm{DOF} = 6(l - n - 1) + \sum_{i=1}^{n} d_i. \tag{5.4}$$

Variable l represents the number of rigid bodies (includes the fixed base) and n is the number of joints. d_i denominates the number of degrees of freedom of joint i. The UPU manipulator presented by [JT03] equation (5.4) generates

$$\mathrm{DOF}_{\mathrm{UPU}} = 6(5 - 6 - 1) + 6 \cdot 2 = -12 + 12 = 0. \tag{5.5}$$

That means the delta mechanism has no degree of freedom. Hence the moving platform is not able to move by oneself. Only the driven prismatic joints offer the mobility for the required degree of freedom.[CYX13]

For the adjustment system of the radio telescope the prismatic joints respectively the linear actuators can be located in the tripod legs. That means replacing an immovable part of the tripod structure with an actuator of variable length on each leg. Since the drives are integrated in the former rigid tripod the external dimensions should not change significantly. Thus a big advantage of this arrangement is the expectable low additional shading of the reflector surface.

With the presented architecture it is not possible to realize the desired rotational movement of the primary antenna. An additional actuator is needed. Because this motion is dedicated to the issue of the polarization it is reasonable to place this additional degree of freedom at the end of the kinematic chain. Therewith the rotation does not superimpose the translational movement. So, the mechanism in figure 5.4 is extended with the rotary drive upon the moving platform to rotate the end–effector.

This concept requires a redesign of the tripod structure. A the lower end the pivots only offer one rotatory degree of freedom. They have to be replaced by universal joints. Each needs to be strong enough to support one tripod leg and partly the weight of the feed horn. Furthermore This collides with the request for no changes on the existing telescope structure.

Placing the linear actors in the structure of the tripod adds an additional supporting task to them. They have to assure the static rigidity of the tripod. This imposes axial as well as lateral forces to the actuators. Any lateral strain is not the intended working direction and has to be considered in the design phase.

5.2.3 Delta mechanism as a stand-alone unit

The disadvantage of the integrated delta mechanism is the bad maintainability and exchangeability of the system. The consolidation of the tripod with the delta robot

induces the impossibility of a discrete view on two separated systems. With regard to the installation and maintenance effort a division of the functions appears to be worthwhile. Leaving the tripod structure unaffected could mean to install a delta mechanism as an independent system. This can be mounted to the bearings of the three tripod legs shown in figure 5.2. To provide an unblocked path of rays between the feed horn and the reflector surface the presented UPU-manipulator from figure 5.4 is turned around with the fixed base at the top. The former movable platform is the mounting for the antenna feed. Just as in the integrated delta mechanism the rotatory motion has to be added. Added as a serial actuation a suitable rotary drive can be placed upon the moving platform to avoid the unwanted superposition with the delta-robot movements.

This design delivers a compact system without any peripheral actuation outside the constructed space. The component can be mounted on the bearings of the tripod structure leaving the rest of the telescope unaffected.

5.2.4 Stewart-Gough-Platform

The Stewart-Gough-Platform is a widely known parallel mechanism. It offers six degrees of freedom. That allows a much higher flexibility for any future adjustment or calibration requirement than the presented delta mechanisms.

Even though this design offers a degree of freedom equal to six and exceed M06 and M07, the rotatory motion around the vertical axis is not fulfilled sufficiently. Obviously a rotation with $\geq 180°$ is not possible with this mechanism. So an additional rotary drive is needed at the moving platform.

5.2.5 Delta robot with rotary drive

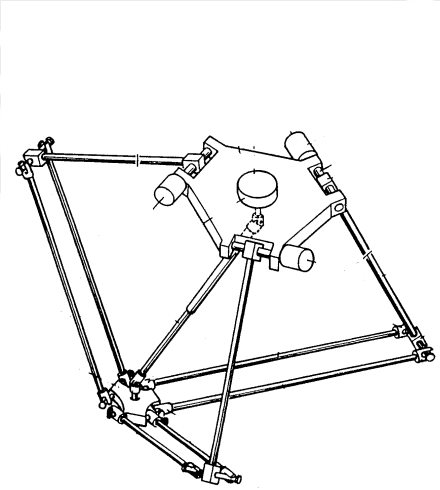

Figure 5.5: Delta–robot with rotatory drives supplemented by a telescopic cardan shaft from [Cla91]

In the year 1991 Clavel discussed in [Cla91] a parallel–manipulator with exclusively rotatory drives. Figure 5.5 shows the concept. The mechanism consists of three limbs linked to a fixed base and a moving platform. The arms are arranged around the fixed based with an angle of 120 ° between each other. Each arm consists of two rigid bodies linked with a spherical joint (DOF = 3). The moving platform is coupled through the kinematic chains of the three limbs to the fixed base. The structure of the forearms with four spherical joints and the rigid bodies forms a parallelogram. Due to this construction the three rotations are eliminated and the moving platform restricted to three translational movements. So this allows only motions with the platform parallel to the fixed base. Clavel mentioned in [Cla90] an idea to add a rotational degree of freedom using a telescopic cardan shaft between the base plate and the end-effector. With this additional freedom the required movements from *M06* and *M07* are possible. Furthermore this sets no limits to the angle of rotation around the vertical axis.

5.3 Selection and evaluation of the actuation principles

To compare the presented principles and provide a less subjective assessment some specific factors from the general requirements will be chosen and weighted. For this standard of evaluation every principle will be reviewed and rated. The criteria are chosen by their ability to compare the concepts and their importance. Furthermore they have to be independent from each other to allow a mostly uncorrelated assessment of each factor.

In the end there are five design concepts to compare:

- TP1 - serial actuation
- TP2 - integrated 3-UPU-delta-robot
- TP3 - stand-alone 3-UPU-delta-robot-unit
- TP4 - Stewart-Gough-Platform
- TP5 - delta robot with rotatory drive

All concepts have to fulfil the fundamental requirements of the table 5.1. Hence only criteria with a range of conformance are suitable for a comparison. For the intended working environment an important fact is the *robustness* of the system. A small quantity of pieces reduces the effort to protect sensitive parts. Also exposed bearings weak the robustness of the system and may require additional housing. This would augment the demand of *space*. This is a factor to reduce to avoid additional and unwanted shading of the reflector surface. This would decrease the overall antenna gain and has to be prevented. The actuation system is intended to improve the performance of the telescope while offering an adjustable feed. Some actuation principle has an augmented working space caused by its design. This is taken into account as a positive characteristic. Its greater working space is counted as higher *flexibility*. In future work or for any calibration for instance this could be an advantage. The *effort to maintain*

criteria	robustness	space / shading	flexibility	maintenance effort	weight	costs	sum	percentage
robustness	x	1	2	1	0	2	6	20.00
space / shading	1	x	2	2	1	2	8	26.67
flexibility	0	0	x	1	0	1	2	6.67
maintenance effort	1	0	1	x	0	1	3	10.00
weight	2	1	2	2	x	2	9	30.00
costs	0	0	1	1	0	x	2	6.67

Table 5.2: Weighting matrix

the actuation system should be as small as possible. For a system independently from other parts of the telescope and a small number of critical components the maintenance is much easier. Since the telescope is designed to be preferably light to reduce the deformations due to its own weight, the *mass* of the actuation system should be small. In particular at the head of the tripod with its slim legs an heavy actuation system is inappropriate. At the end also economical aspects like the *costs* of the system will be estimated and rated.

As criteria for the assessment are chosen

- robustness
- demand of space / shading
- flexible application
- maintenance effort
- weight
- costs

To consider the importance and impact of every criteria, the factors are weighed amongst each other. Table 5.2 shows the weighting matrix. Each criteria is rated against all others with three levels. Zero 0 means that the actual issue (row) is less important than the correspondent one in the column. One 1 denominates a balanced importance while 2 is given in case of a more important factor. The values from each row are summarized and set in relation to each other. The last column shows the weight of every criteria in a row in comparison to the others.

Table 5.3 shows the evaluation of all technical concepts TP1 to TP5. Every concept is rated in matter of each of the six criteria with a score from 1 to 5 with 5 as the best

		TP1		TP2		TP3		TP4		TP5	
	W	R	WR	R	WR	R	WR	R	WR	R	WR
robustness	0.2000	3	0.600	4	0.800	5	1.000	3	0.600	4	0.800
space / shading	0.2667	1	0.267	5	1.333	4	1.067	3	0.800	4	1.067
flexibility	0.0667	1	0.067	3	0.200	4	0.267	5	0.333	4	0.267
maintenance effort	0.1000	3	0.300	1	0.100	5	0.500	4	0.400	4	0.400
weight	0.3000	1	0.300	5	1.500	4	1.200	2	0.600	4	1.200
costs	0.0667	4	0.267	3	0.200	4	0.267	2	0.133	4	0.267
sum			1.80		4.13		4.30		2.87		4.00

Table 5.3: Assessment of the design concepts

grade for the best fulfilment. Each grade R is multiplied with the criteria weight W. The sum of all weighted grades is the value to compare the designs. Concept *TP3* gets the highest value.

5.4 Preliminary design and construction

5.4.1 Selection of components and assembly

Mount to tripod and base frame

To construct concept TP3 a base frame is needed. This stand is intended to be the fundament for the delta mechanism. The base frame will be mounted on the top of the tripod. For this the tripod provides three connecting points. A preliminary dummy mount was shown in figure 5.2. So the existing concept of the bearings will be used. Since there are three mounting points to the tripod with an angle of 120 ° between and three for the delta mechanism arranged in the same angle, an hexagonal set-up can be an appropriate design. This layout is shown in figure 5.7.

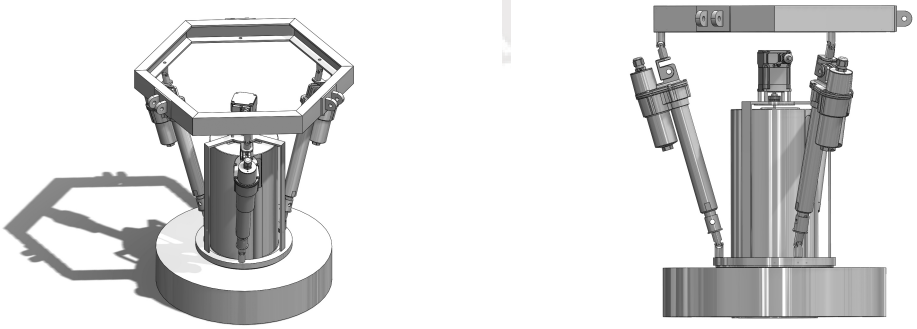

Figure 5.6: Preliminar assembly with 1420 MHz-feed

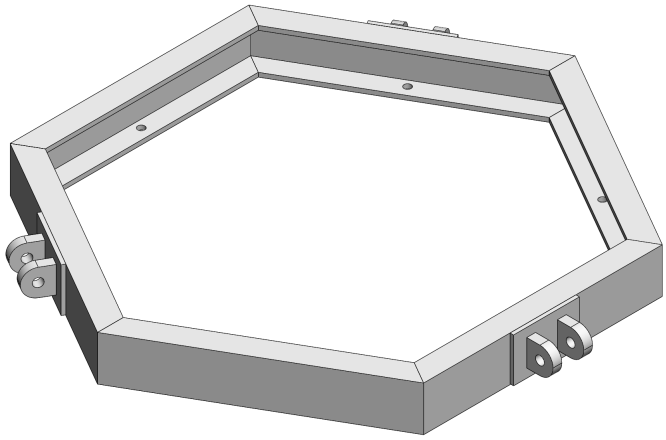

Figure 5.7: Hexagonal base frame with bearings to the tripod

The hexagon is composed by six U-profiles from *Aceros Arequipa* to engage the same supplier as contracted to deliver the bars for the telescope structure. A roughly dimensioning was made assuming a simple two-dimensional load case with a force affecting at the middle of a bar. The size delivers a stiffness more than required.

Universal joints

The universal joints are intended to provide two rotatory motions. Universal joints are used in cardan shafts and therefore also named as cardan joints. In contrast to spherical joints they suppress one rotation to allow the transmission of a torque. For the actual work they will be used to restrain the articulation to two rotations without revolving around the vertical axis. Three universal joints have to be mounted at the base frame. The other ones are attached to the moving platform.on one side and bearing a linear actor at the other side.

Linear actuators

The most important characteristic of the linear actuators is the possible stroke. The actuators are working as driven prismatic joints. For a given geometry of the delta mechanism, the equation (5.10) delivers the generalized coordinates q_i for every actuator. The force of 30 lb is enough taking in account the three actuators always acting simultaneously. Using the linear drive with the optional worm screw provides a self-locking gear. This is fulfils *F02* without any additional construction.

For the selection of the actuators, the resistance against environmental influences is an important criteria. The selected *Max Jac* drives from *Thomson* (see appendix 6)

providing a protection class IP66. Following the specification they withstand any expectable pollution and humidity at the intended working site in Lima. The housing is hard coat anodized to assure a high resistance to corrosion.

The actuator can handle electric power supplies offering 12 as well as 24 V DC. The infrastructure of the telescope provides this, so this complies with the requirement *F23*. For the control the selected actuators provide a position feedback signal from an integrated encoder.

Drive for the rotary motion

The rotatory motion is realized subsequent to the delta mechanism by an independent rotation unit. A rack mounted upon the delta–actuated ring encases the feed–adapter. The rotary drive is located on top of the frame followed by an axial bearing. This is required to meet the expected high axial load due to the weight of the antenna feed. To compensate the induced force and avoid stress to the motor, the axial bearing has to support the whole antenna feed.

5.4.2 Examination of the inverse kinematics

General deviation

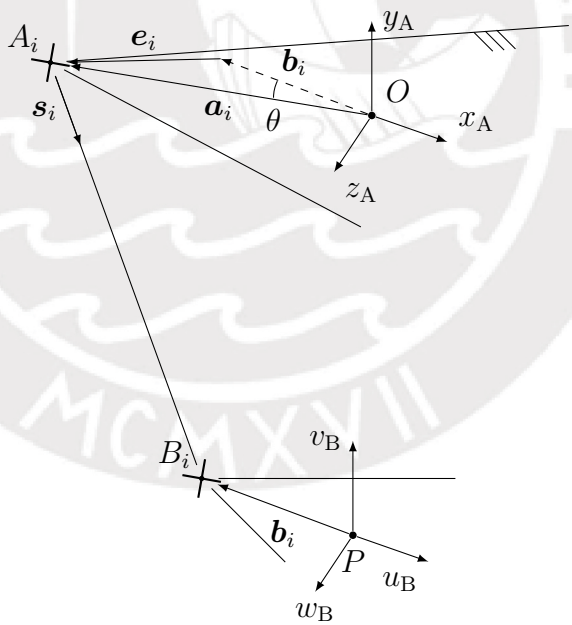

Figure 5.8: Limb i of the delta mechanism mounted to the tripod – adapted from [JT03]

Figure 5.8 shows limb i of the 3–UPU–mechanism. The coordinate system A with $x_\mathrm{A}y_\mathrm{A}z_\mathrm{A}$ is dedicated to the base frame fixed to the tripod and pinned to point O.

The moving platform is located below and handled by the coordinate system B with $u_\mathrm{B} v_\mathrm{B} w_\mathrm{B}$. The calculation of the inverse kinematics is related to the reference point P on the moving platform. Limb i is linked via A_i to the base frame and B_i to the moving platform. The points A_i for $i = 1, 2, 3$ lie on the $x-z$–plane in a distance of r_a from point O and accordingly B_i with the $u-w$ plane and the distance r_b from point P. Coordinate system B is positioned such that the axes u and w are parallel to x and z in A. The orientation of the moving platform in relation to the base frame always remains constant. So the vector ${}^\mathrm{B}\boldsymbol{b}_i$ in coordinate system B is equal to ${}^\mathrm{A}\boldsymbol{b}_i$ in A. [JT03]

So the two position vectors $\boldsymbol{a}_i$ and $\boldsymbol{b}_i$ consist of

$$\boldsymbol{a}_i = \begin{pmatrix} a_{i\mathrm{x}} & 0 & a_{i\mathrm{z}} \end{pmatrix}^\top \tag{5.6}$$

$$\boldsymbol{b}_i = \begin{pmatrix} b_{i\mathrm{x}} & 0 & b_{i\mathrm{z}} \end{pmatrix}^\top . \tag{5.7}$$

The length q_i of the limb and generalized coordinate for the linear actuator points along $\boldsymbol{s}_i$ and can be expressed by the vector-loop

$$\boldsymbol{q}_i = q_i \boldsymbol{s}_i = \boldsymbol{p} + \boldsymbol{b}_i - \boldsymbol{a}_i. \tag{5.8}$$

The two constant vectors $\boldsymbol{b}_i$ and $\boldsymbol{a}_i$ can be merged to the constant $\boldsymbol{e}_i = \boldsymbol{a}_i - \boldsymbol{b}_i$. Squaring equation (5.8) delivers

$$\boldsymbol{q}_i^2 = \left[\boldsymbol{p} - \boldsymbol{e}_i\right]^\top \left[\boldsymbol{p} - \boldsymbol{e}_i\right]. \tag{5.9}$$

This has the two solutions

$$\boldsymbol{q}_i = \pm\sqrt{\left(p_\mathrm{x} - e_{i\mathrm{x}}\right)^2 + p_\mathrm{y}^2 + \left(p_\mathrm{z} - e_{i\mathrm{z}}\right)^2} \tag{5.10}$$

whereof the negative solution can be discarded because of the impossibility of such a length of a limb. The inverse kinematics can be expressed by equation (5.10). It is possible to calculate the stroke of each linear actuator for the position vector $\boldsymbol{p}$ and so for the location of the moving platform. [JT03]

Implementation for the present actuation system

To apply equation (5.10) to the actual actuation system, the vector $\boldsymbol{e}_i$ requires the knowledge about the geometry of the assembly. Regarding this, the assembly shown in figure 5.6 was measured. Vector $\boldsymbol{e}_i$ is composed by the coordinates of the connection points as

$$\boldsymbol{e}_i = \begin{pmatrix} a_{i\mathrm{x}} \\ a_{i\mathrm{y}} \\ a_{i\mathrm{z}} \end{pmatrix} - \begin{pmatrix} b_{i\mathrm{x}} \\ b_{i\mathrm{y}} \\ b_{i\mathrm{z}} \end{pmatrix} \tag{5.11}$$

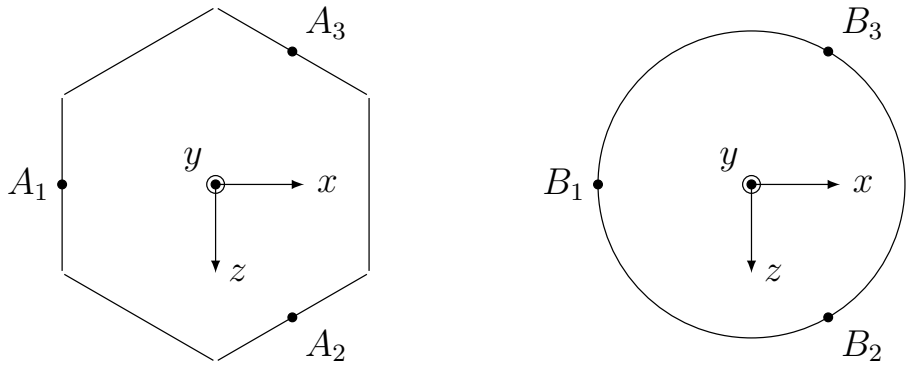

(a) Base frame (b) Moving platform

Figure 5.9: Orientation of the UPU-mechanism in terms of (xyz)-coordinates

So, with figure 5.9 and the measurement of the vectors $\boldsymbol{a}_i$ and $\boldsymbol{b}_i$ in the model in SolidWorks, the matrix $\boldsymbol{E} = [\boldsymbol{e}_1\ \boldsymbol{e}_2\ \boldsymbol{e}_3]$ can be written as

$$\boldsymbol{E} \approx \begin{pmatrix} -113.16 & 56.58 & 56.58 \\ 0 & 0 & 0 \\ 0 & -98 & 98 \end{pmatrix}. \tag{5.12}$$

With the knowledge of the geometry-matrix $\boldsymbol{E}$, the required stroke of the linear actuators can be determined. The required minimum working space is set by table 5.1. Thus the equation (5.10) can be used to determine the minimum stroke for the drives. The reference point P with its coordinates p_x, p_y and p_z has to perform the displacement derived as the offset from section 4.3. For any maximum value of y_{off} or x_{off} (z is neglected) none of the q_i extends 150 mm. So, for the chosen linear actors from *Thomson* the model with 150 mm can be selected.

CHAPTER 6

Conclusion and prospect

This work has shown a possibility to estimate the homologous reflector deformation of the INRAS RT–20 due to its own weight. Based on this, a recommendation for an actuation system to refocus the primary antenna is presented.

Based on an existing line model, a structural model of the reflector backing structure for a finite-element simulation in ANSYS has been developed. For the simulation of the reflector deformation due to its own weight a load case was generated. This scenario was simulated for changing elevation angles. The result of the simulation consists of position vectors of the points representing the reflector surface. For reproducibility and fast execution this process was automatized in APDL–scripts. The scripts run the simulations automatically while printing the results into text-files.

For the deformed reflector surface, a mathematical description was derived. Several optimization methods are implemented in MatLab to determine fitting-curves for the point clouds produced by the simulation. The results and methods were compared and evaluated regarding the residual RMS–error of the surface fittings. With the mathematical description of the deformed reflector the position of the new focal point is determined. The output is compared with the expectations arised from the homologous design. With this a potential corrective movement of the primary antenna was derived.

For the construction of an actuation system to refocus the telescope several technical concepts to adjust the primary antenna were discussed. The ideas of the VDI2221–norm supported the methods of the development process and the assessment. One suitable technical solution was elected and explored in more detail to provide a preliminary design and a prototype as a CAD–model.

There are several programs, scripts and digital models attending this thesis:

- ANSYS APDL–scripts to convert the line model of the RT–20 into a well-defined structural model for a finite–element analysis
- ANSYS APDL–scripts to create load cases for the simulation of the dead-weight-deformation of the telescope in different elevation angles
- MatLab–scripts to find the parameters for a best-fitting paraboloid in a point cloud provided by ANSYS output-files
- Look-Up-Tables for the dead-weight deformation
- SolidWorks-CAD-assemblies and components for the actuation system
- corresponding data sheets for purchased parts

This work estimates the deformations due to gravity in different elevation angles. There are influences by temperature and wind loads as well. These are discussed in chapter 2.1 but not further examined. For a full analysis, a future work has to implement this simulations in ANSYS.

The INRAS RT–20 radio telescope is under construction. The reflector surface could not be implemented in the model of the simulation. Therefore in section 4.1.1 several assumptions and approximations have been made to allow further investigations. Regarding to this, there is a residual but small error in the fitting–algorithm.

The knowledge about the deformations of the reflector surface and the misalignment between the focal point and the primary antenna were determined theoretically. Today it is not possible to prove the predictions of this work at reality. Not before the telescope goes into operation, the results can be verified by measurements.

List of Figures

List of Tables

Bibliography

[ASC06] ASCE: *Minimum design loads for buildings and other structures*. 2006

[AZ88] Acosta, Roberto J. ; Zaman, Afroz A.: Analytical approximation of a distorted reflector surface defined by a discrete set of points / Antenna Application Symposium. 1988. – Forschungsbericht

[AZK+94] Antebi, Joseph ; Zarghamee, M ; Kan, Frank W. ; Hartwell, Haywood ; Salah, Joseph E. ; Milner, Steve M.: A deformable subreflector for the Haystack radio telescope. In: *Antennas and Propagation Magazine, IEEE* 36 (1994), Nr. 3, S. 19–28

[Baa07] Baars, Jacob W.: *The paraboloidal reflector antenna in radio astronomy and communication*. Springer, 2007

[Bal05] Balanis, A. C.: *Antenna theory: analysis and design*. 3. John Wiley, 2005

[Bär13] Bär, Gert: *Geometrie: eine Einführung in die analytische und konstruktive Geometrie*. Springer-Verlag, 2013

[BBI02] Brenner, Michael ; Britcliffe, Michael J. ; Imbriale, W: Gravity deformation measurements of 70 m reflector surfaces. In: *IEEE Antennas & Propagation Magazine* 44 (2002), Nr. 6, S. 187–192

[BGS02] Burke, Bernard F. ; Graham-Smith, Francis: *An introduction to radio astronomy*. Cambridge University Press, 2002

[BHL+08] Bronstein, Ilja N. ; Hromkovic, Juraj ; Luderer, Bernd ; Schwarz, Hans-Rudolf ; Blath, Jochen ; Schied, Alexander ; Dempe, Stephan ; Wanka, Gert ; Gottwald, Siegfried ; Zeidler, Eberhard u. a.: *Taschenbuch der Mathematik*. Bd. 1. Harri Deutsch, 2008

[Bir11] Bird, Trevor S.: Feed Antennas. In: Balanis, Constantine A. (Hrsg.): *Modern antenna handbook*. John Wiley & Sons, 2011, Kapitel 18, S. 867–927

[BSGN04] Borovkov, Alexey I. ; Shevchenko, Denis V. ; Gaev, Alexander V. ; Nemov, Alexander S.: 3D Finite Element Thermal and Structural Analysis of the RT-70 Full-Circle Radio Telescope. In: *Proceedings of International ANSYS Conf*, 2004

[BZKY11] Binbin, Peng ; Zengming, Li ; Kai, Wu ; Yu, Sun: Kinematic Characteristics of 3-UPU Parallel Manipulator in Singularity and Its Application. In: *Intec Journal of Advanced Robotic Systems* 8 (2011), Nr. 4, S. 54–64

[CB10] Coleman, Michael J. ; Baginski, Frank: A shape deformation study of large aperture inflatable elastic parabolic antenna reflectors. In: *Proceedings of the 51st AIAA/ASME/AHS/ASC Structures, Structural Dynamics, and Materials Conference, Orlando, FL*, 2010

[CH69] Christiansen, Wilbur N. ; Högbom, Jan A.: *Radiotelescopes*. Cambridge University Press, 1969

[Cla90] Clavel, Reymond: *Device for the Movement and Positioning of an Element in Space*. `http://www.google.com/patents/US4976582`. Version: Dezember 11 1990. – US Patent 4,976,582

[Cla91] Clavel, Reymond: *Conception d' un robot parallèle rapide à 4 degrés de liberté*, Ecole Polytechnique Federale de Lausanne, Diss., 1991

[Cle04] Cleve, Moler: *Numerical Computing with Matlab*. Society for Industrial and Applied Mathematics, 2004

[CYX13] Chang, Wen W. ; Yusup, Ai L. ; Xiang, Bin B.: A New Best-Fit Method for Distorted Reflector Antenna Surface. In: *Applied mechanics and materials* 2491 (2013), Nr. 336, S. 1857–1862

[FHY+13] Franco, Rosendo ; Heraud, Jorge ; Yépez, Herbert ; Chambergo, José ; Carrasco, Cristian ; Coveñas, José L. ; Verástegui, Ernesto E. ; Arce, Carla ; Centa, Víctor ; Carrero, Felipe: Análisis por Elementos Finitos de Esfuerzos y Deformaciones de las Estructuras Principales de un Radiotelescopio de 20 Metros de Diámetro. In: Franco, Rosendo (Hrsg.) ; Valverde, Quino (Hrsg.) ; Yépez, Herbert (Hrsg.) ; Carrasco, Cristian (Hrsg.): *CAIP 2013* 11° *Congreso Interamericano de Computación Aplicada a la Industria de Procesos* Bd. 11. Lima, Octubre 2013

[Gaw04] Gawronski, Wodek: Control and pointing challenges of antennas and (Radio) telescopes. In: *IPN Progress Report* (2004), S. 42–159

[Gaw08] Gawronski, Wodek: *Modeling and Control of Antennas and Telescopes*. Springer Science & Business Media, 2008

[GBP+05] Greve, Albert ; Bremer, Michael ; Penalver, Juan ; Raffin, Philippe ; Morris, David: Improvement of the IRAM 30-m telescope from temperature measurements and finite-element calculations. In: *Antennas and Propagation, IEEE Transactions on* 53 (2005), Nr. 2, S. 851–860

[GNS98] Greve, A ; Neri, R ; Sievers, A: The gain–elevation correction of the IRAM 30–m telescope. In: *Astronomy and Astrophysics supplement series* 132 (1998), Nr. 3, S. 413–416

[HEH89] Hills, R.E. ; Edwards, B.W.H. ; Hall, J.E.: Aspects of the design of the James Clerk Maxwell Telescope. In: *Mechanical Aspects of Antenna Design, IEE Colloquium on*, 1989, S. 3/1–3/4

[Hey72] Heyer, Ernst ; Dietrich, Christine (Hrsg.): *Witterung und Klima*. 6. Leipzig : Teubner Verlagsgesellschaft, 1972

[HFA+14] Heraud, Jorge A. ; Franco, Rosendo ; Arce, Carla A. ; Carrero, Felipe E. ; Centa, Victor A.: RT-20, the 20 meter diameter radio telescope in Lima, Peru. In: *URSI General Assembly and Scientific Symposium. International Union of Radio Science, Beijing* 31 (2014)

[HK92] Hall, Robert ; King, Lee J.: The Green Bank Telescope. In: *Antennas and Propagation Society International Symposium, 1992. AP-S. 1992 Digest. Held in Conjuction with: URSI Radio Science Meeting and Nuclear EMP Meeting., IEEE* IEEE, 1992, S. 862–865

[HK11] Holst, Christoph ; Kuhlmann, Heiner: *Bestimmung der elevationsabhängigen Deformation des Hauptreflektors des 100m-Radioteleskops Effelsberg mit Hilfe von Laserscannermessungen*. Dec 2011

[Hoe67a] Hoerner, Sebastian: Design of large steerable antennas. In: *The Astronomical Journal* 72 (1967), S. 35

[Hoe67b] Hoerner, Sebastian: Homologous deformations of tiltable telescopes. In: *J. Structural Division Proc. ASCE* 93 (1967), S. 461–486

[Hoe68] Hoerner, Sebastian: *A Steerable 300-foot Telescope for 2 cm Wavelength*. Addendum, Apr 1968. – LFST Report No. 4

[HW75] Hoerner, Sebastian ; Wong, Woon-Yin: Gravitational deformation and astigmatism of tiltable radio telescopes. In: *Antennas and Propagation, IEEE Transactions on* 23 (1975), Nr. 5, S. 689–695

[IBB01] Imbriale, WA ; Britcliffe, MJ ; Brenner, M: Gravity Deformation Measurements of NASA's Deep Space Network 70-Meter Reflector Antennas. In: *The Inter-Planetary Network Progress Report 42-147, July–September 2001* (2001), S. 1–15

[IJ07] Imbriale, William A. ; Jones, Dayton L.: Radio-telescope antennas. Version: 4, 2007. `https://books.google.de/books?id=bmdFAAAAYAAJ`. In: Volakis, John L. (Hrsg.): *Antenna Engineering Handbook, Fourth Edition*. 4. McGraw-Hill Companies, 2007. – ISSN 1063–665X, Kapitel 49

[Imb11] Imbriale, William A.: Reflector Antennas. In: Balanis, Constantine A. (Hrsg.): *Modern Antenna Handbook*. Wiley, 2011, Kapitel 5, S. 201–262

[JJB+12] Joffe, R. ; Jēkabsons, N. ; Bērziņš, A. ; Klapers, M. ; Upnere, S.: Evaluation Of Damage And Deformation Of Rt-32 Radio Telescope / Radioteleeskopa Rt-32 Deformācijas Un Bojājumu Novērtējums. In: *Latvian Journal of Physics and Technical Sciences* 49 (2012), Dezember, S. 4–12. `http://dx.doi.org/10.2478/v10047-012-0037-x`. – DOI 10.2478/v10047–012–0037–x

[JT03] Joshi, Sameer ; Tsai, Lung-Wen: A Comparison Study of Two 3-DOF Parallel Manipulators: One With Three and the Other With Four Supporting Legs. In: *IEEE Transactions on Robotics and Automation* 19 (2003), April, Nr. 2, S. 200–209

[Kat70] Katow, MS: Antenna Structures: Evaluation of Reflector Surface Distortions. In: *The Deep Space Network Progress Report* (1970), S. 76–80

[KCC87] Kiedron, K ; Chian, CT ; Chuang, KL: Statistical analysis of the 70 meter antenna surface distortions. (1987)

[Kit90] Kitsuregawa, Takashi: Advanced technology in satellite communication antennas: electrical and mechanical design. In: *Norwood, MA, Artech House, 1990, 429 p.* 1 (1990)

[KKN+07] Kaiden, Masahiro ; Kimura, Kimihiro ; Nakajima, Taku ; Tokko, Yoshihide ; Tsuji, Kiyoko ; Okuno, Hirofumi ; Kojima, Takafumi ; Hara, Kazuyoshi ; Abe, Yasuhiro ; Yonekura, Yoshinori u. a.: Development of the main reflector and optics for the 1.85 m millimeter radio telescope. In: *Proceedings of ISAP2007, Niigata, Japan*, 2007, S. 916–918

[KL13] Kalinin, AV ; Leschev, SS: Compensation of gravitational deformations of large reflector antennas using radio holography. In: *Antenna Theory and Techniques (ICATT), 2013 IX International Conference on* IEEE, 2013, S. 429–430

[Kra93] Kraus, John D.: Radio-Telescope Antennas. In: Johnson, Richard C. (Hrsg.): *Antenna Engineering Handbook*. 3. McGraw-Hill Companies, 1993, Kapitel 41

[LAMV04] Legg, TH ; Avery, Lorne W. ; Matthews, Henry E. ; Vallee, Jacques P.: Gravitational deformation of a reflector antenna measured with single-receiver holography. In: *Antennas and Propagation, IEEE Transactions on* 52 (2004), Nr. 1, S. 20–25

[Lev94] Levy, Roy: Structural Engineering of Microwave Antennas, Chapters 1-4. (1994)

[Lou05] Lourakis, Manolis I.: A brief description of the Levenberg-Marquardt algorithm implemented by levmar. In: *Foundation of Research and Technology - Hellas* 4 (2005), S. 1–6

[Lue10] Lueger, Otto: *Lexikon der gesamten Technik und ihrer Hilfswissenschaften*. Bd. 8. 2. Stuttgart : Deutsche Verlagsanstalt, 1910

[LWH14] Lian, Peiyuan ; Wang, Wei ; Hu, Naigang: Feed adjustment method of reflector antenna based on far field. In: *Microwaves, Antennas & Propagation, IET* 8 (2014), Nr. 10, S. 701–707

[Mat14] MathWorks: *MATLAB R2014a Dokumentation*. `http://www.mathworks.com/help/index.html`. Version: 2014

[Mer06] Merlet, Jean-Pierre: *Parallel robots*. Bd. 128. 2nd. Springer Science & Business Media, 2006

[MG07] Müller, Günter ; Groth, Clemens: *FEM für Praktiker: Grundlagen: Basiswissen und Arbeitsbeispiele zu FEMAnwendungen; Lösungen mit dem Programm ANSYS Rev. 9/10; mit zahlrreichen Beispielen auf CD-ROM/Günter Müller/Clemes Groth*. 8. expert verlag, 2007

[NPEH10] Nothnagel, Axel ; Pietzner, Judith ; Eling, Christian ; Hering, Claudia: Homologous Deformation of the Effelsberg 100 m Telescope determined with a Total Station. In: *Sixth International VLBI Service for Geodesy and Astronomy. Proceedings from the 2010 General Meeting,* Bd. 1, 2010, S. 123–127

[RS07] Rahmat-Samii, Yahya: Reflector Antennas. In: Volakis, John L. (Hrsg.): *Antenna Engineering Handbook*. 4. McGraw-Hill Companies, 2007, Kapitel 15

[Ruz65] Ruze, J.: Lateral-feed displacement in a paraboloid. 13 (1965), Nr. 5, 660–665. `http://dx.doi.org/10.1109/TAP.1965.1138514`. – DOI 10.1109/TAP.1965.1138514

[Ruz66] Ruze, John: Antenna tolerance theory–a review. In: *IEEE Proceedings* Bd. 54, 1966, S. 633–642

[Spä01] Späth, Helmuth: Least squares fitting with rotated paraboloids. In: *Mathematical Communications* 6 (2001), Nr. 2, S. 173–179

[Sub05] Subrahmanyan, Ravi: Photogrammetric measurement of the gravity deformation in a Cassegrain antenna. In: *Antennas and Propagation, IEEE Transactions on* 53 (2005), Nr. 8, S. 2590–2596

[TJ00] Tsai, Lung-Wen ; Joshi, Sameer: Kinematics and optimization of a spatial 3-UPU parallel manipulator. In: *Journal of Mechanical Design* 122 (2000), Nr. 4, S. 439–446

[UJJ+11] Upnere, Sabine ; Jekabsons, Normunds ; Joffe, Roberts ; Bezrukovs, Valerijs ; Bezrukovs, Vladislavs: Analysis of wind influence to radio astronomy observations at Irbene radio-telescope complex. In: *Scientific Journal of Riga Technical University. Environmental and Climate Technologies* 6 (2011), Nr. 1, S. 118–126

[UJJ12a] Upnere, Sabine ; Jekabsons, Normunds ; Joffe, Roberts: Characterization of Wind Loading of the Large Radio Telescope. In: *Boundary Field Problems and Computer Simulation* 54 (2012), S. 30–37

[UJJ12b] Upnere, Sabine ; Jekabsons, Normunds ; Joffe, Roberts: Development of Mechanical Models of RT-16 and RT-32 Radio Telescopes. In: *Space Research Review* 1 (2012), S. 112–125

[UJJ13] Upnere, S ; Jekabsons, N ; Joffe, R: Numerical Analysis of Large Telescopes in Terms of Induced Loads and Resulting Geometrical Stability. In: *Journal of Theoretical and Applied Mechanics* 43 (2013), Nr. 1, S. 39–46

[VDI93] VDI: *VDI 2221 Methodik zum Entwickeln und Konstruieren technischer Systeme und Produkte*. Düsseldorf, 1993

[VDI04] VDI: *VDI 2206 Entwicklungsmethodik für mechatronische Systeme*. Düsseldorf, 2004

[VSA04] Vogiatzis, Konstantinos ; Segurson, Anna ; Angeli, George Z.: Estimating the effect of wind loading on extremely large telescope performance using computational fluid dynamics. In: *SPIE Astronomical Telescopes+ Instrumentation* International Society for Optics and Photonics, 2004, S. 311–320

[WD07] Wang, Wei ; Duan, Baoyan: Gravity Deformation and Gain Loss of 12m Reflector Antenna. In: *Mechatronics and Automation, 2007. ICMA 2007. International Conference on* IEEE, 2007, S. 927–931

[WDQ+04] Wang, CS ; Duan, BY ; Qiu, YY u. a.: A new approach to fit the distorted reflector antenna and its computation of electrical characteristics. In: *The First Asia International Symposium on Mechatronics (AISM'2004), Xi'an, China*, 2004, S. 27–30

[WK95] Wells, Donald C. ; King, Lee: Gbt best-fitting paraboloid [bfp] in c. In: *NRAO GBT Memo Series* 131 (1995)

[WLL10] Wang, W ; Leng, GJ ; Li, HP: Subreflector real-time compensation for main reflector deformation of shaped Cassegrain antenna. In: *PIERS Proceedings*, 2010, S. 42–46

[WVS94] Woody, DAVID ; Vail, DAVID ; Schaal, WALTER: Design, construction, and performance of the Leighton 10.4-m-diameter radio telescopes. In: *Proceedings of the IEEE* 82 (1994), Nr. 5, S. 673–686

[WZZ08] Wang, CS ; Zheng, F ; Zhang, F-S: On divided-fitting method of large distorted reflector antennas based Coons surface. In: *Radar Conference, 2008. RADAR'08. IEEE* IEEE, 2008, S. 1–5

[Yan06] Yang, De-Hua: Structural Design and Analysis of a 50m Fully Steerable Pulsar Radio Telescope. In: *Chinese Journal of Astronomy and Astrophysics* 6 (2006), Nr. S2, S. 324

[YEN98] Yoshikawa, N ; Elishakoff, Isaac ; Nakagiri, S: Worst case estimation of homology design by convex analysis. In: *Computers & structures* 67 (1998), Nr. 1, S. 191–196

[ZLS+11] Zuo, Ying-Xi ; Li, Yang ; Sun, Ji-Xian ; Yang, Ji ; Li, Jing-Jing ; Xu, Ye ; He, Deng-Yun ; Fan, Qin-Hong ; Fan, Sheng-Hong: A Research on the Gravity Deformation of Delingha 13.7 m Telescope. In: *Chinese Astronomy and Astrophysics* 35 (2011), Nr. 4, S. 439–446

[ZZY+12] Zhang, Yong ; Zhang, Jie ; Yang, De-Hua ; Zhou, Guo-Hua ; Li, Ai-Hua ; Li, Guo-Ping: An active reflector antenna using a laser angle metrology system. In: *Research in Astronomy and Astrophysics* 12 (2012), Nr. 6, S. 713

Appendix

Look up tables for the dead weight deformation

Look-up table of the solution by the Backslash-Operator

elevation °	u mm	v mm	w mm	ϕ_x °	ϕ_z °	h 1	D_f mm	x_{off} mm	y_{off} mm	RMSE mm
10	0.00000	−0.48992	0.00000	0.00011	0.01171	−0.00607	44.31951	−3.89496	43.33803	$2.0496E-05$
15	0.00000	−0.48067	0.00000	0.00009	0.01150	−0.00606	44.23870	−3.84598	43.22962	$2.0389E-05$
20	0.00000	−0.47165	0.00000	0.00008	0.01120	−0.00605	44.15972	−3.76770	43.12687	$2.0170E-05$
25	0.00000	−0.46292	0.00000	0.00007	0.01081	−0.00604	44.08322	−3.66073	43.03055	$1.9843E-05$
30	0.00000	−0.45456	0.00000	0.00005	0.01035	−0.00603	44.00975	−3.52593	42.94140	$1.9410E-05$
35	0.00000	−0.44662	0.00000	0.00004	0.00980	−0.00602	43.93987	−3.36425	42.86007	$1.8876E-05$
40	0.00000	−0.43917	0.00000	0.00002	0.00918	−0.00601	43.87416	−3.17702	42.78725	$1.8247E-05$
45	0.00000	−0.43226	0.00000	0.00000	0.00849	−0.00600	43.81304	−2.96554	42.72342	$1.7531E-05$
50	0.00000	−0.42595	0.00000	−0.00001	0.00773	−0.00599	43.75704	−2.73157	42.66910	$1.6740E-05$
55	0.00000	−0.42028	0.00000	−0.00003	0.00692	−0.00598	43.70657	−2.47684	42.62472	$1.5886E-05$
60	0.00000	−0.41530	0.00000	−0.00004	0.00605	−0.00598	43.66200	−2.20313	42.59057	$1.4985E-05$
65	0.00000	−0.41104	0.00000	−0.00006	0.00514	−0.00597	43.62368	−1.91279	42.56694	$1.4057E-05$
70	0.00000	−0.40754	0.00000	−0.00007	0.00419	−0.00597	43.59189	−1.60779	42.55400	$1.3127E-05$
75	0.00000	−0.40483	0.00000	−0.00009	0.00321	−0.00597	43.56687	−1.29058	42.55185	$1.2223E-05$
80	0.00000	−0.40292	0.00000	−0.00010	0.00220	−0.00596	43.54884	−0.96356	42.56052	$1.1383E-05$
85	0.00000	−0.40182	0.00000	−0.00011	0.00117	−0.00596	43.53790	−0.62920	42.57991	$1.0647E-05$
90	0.00000	−0.40156	0.00000	−0.00012	0.00014	−0.00596	43.53416	−0.29005	42.60990	$1.0064E-05$

Look-up table of the solution by the normal equations

elevation °	u mm	v mm	w mm	ϕ_x °	ϕ_z °	h 1	D_f mm	x_{off} mm	y_{off} mm	RMSE mm
10	0,01401	-0,48992	-0,00013	0,00011	0,01166	-0,00607	44,31951	-3,87395	43,33803	2,0496E-05
15	0,01376	-0,48067	-0,00011	0,00009	0,01144	-0,00606	44,23870	-3,82534	43,22962	2,0389E-05
20	0,01340	-0,47165	-0,00010	0,00008	0,01115	-0,00605	44,15972	-3,74760	43,12687	2,0170E-05
25	0,01294	-0,46292	-0,00008	0,00006	0,01076	-0,00604	44,08322	-3,64133	43,03055	1,9843E-05
30	0,01238	-0,45456	-0,00006	0,00005	0,01030	-0,00603	44,00975	-3,50736	42,94140	1,9410E-05
35	0,01172	-0,44662	-0,00004	0,00003	0,00975	-0,00602	43,93987	-3,34666	42,86008	1,8876E-05
40	0,01098	-0,43917	-0,00002	0,00002	0,00914	-0,00601	43,87416	-3,16055	42,78726	1,8247E-05
45	0,01016	-0,43226	0,00000	0,00000	0,00845	-0,00600	43,81304	-2,95030	42,72342	1,7531E-05
50	0,00925	-0,42595	0,00001	-0,00001	0,00770	-0,00599	43,75704	-2,71769	42,66910	1,6740E-05
55	0,00828	-0,42028	0,00003	-0,00003	0,00689	-0,00598	43,70657	-2,46442	42,62472	1,5886E-05
60	0,00724	-0,41530	0,00005	-0,00004	0,00603	-0,00598	43,66200	-2,19227	42,59057	1,4985E-05
65	0,00615	-0,41104	0,00007	-0,00006	0,00512	-0,00597	43,62368	-1,90357	42,56694	1,4057E-05
70	0,00501	-0,40754	0,00009	-0,00007	0,00417	-0,00597	43,59189	-1,60027	42,55400	1,3127E-05
75	0,00384	-0,40483	0,00010	-0,00009	0,00319	-0,00597	43,56687	-1,28483	42,55185	1,2223E-05
80	0,00263	-0,40292	0,00012	-0,00010	0,00219	-0,00596	43,54884	-0,95962	42,56052	1,1383E-05
85	0,00140	-0,40182	0,00014	-0,00011	0,00117	-0,00596	43,53790	-0,62709	42,57991	1,0647E-05
90	0,00017	-0,40156	0,00015	-0,00012	0,00014	-0,00596	43,53416	-0,28980	42,60990	1,0064E-05

Look-up table of the solution by the cftool

elevation °	u mm	v mm	w mm	ϕ_x °	ϕ_z °	h 1	D_f mm	x_{off} mm	y_{off} mm	RMSE mm
10	0,01417	-0,48992	-0,00013	0,00011	0,01165	-0,00607	44,31951	-3,87371	43,33803	3,4791E-04
15	0,01414	-0,48067	-0,00010	0,00009	0,01144	-0,00606	44,23870	-3,82476	43,22962	3,4609E-04
20	0,01311	-0,47165	-0,00010	0,00008	0,01115	-0,00605	44,15972	-3,74804	43,12687	3,4238E-04
25	0,01280	-0,46292	-0,00009	0,00006	0,01076	-0,00604	44,08322	-3,64153	43,03055	3,3683E-04
30	0,01253	-0,45456	-0,00006	0,00005	0,01030	-0,00603	44,00975	-3,50713	42,94140	3,2948E-04
35	0,01191	-0,44662	-0,00004	0,00003	0,00975	-0,00602	43,93987	-3,34639	42,86008	3,2041E-04
40	0,01119	-0,43917	-0,00002	0,00002	0,00914	-0,00601	43,87416	-3,16023	42,78726	3,0973E-04
45	0,01006	-0,43226	0,00000	0,00000	0,00845	-0,00600	43,81304	-2,95044	42,72342	2,9758E-04
50	0,00913	-0,42595	0,00002	-0,00001	0,00770	-0,00599	43,75704	-2,71787	42,66910	2,8415E-04
55	0,00827	-0,42028	0,00003	-0,00003	0,00689	-0,00598	43,70657	-2,46443	42,62472	2,6965E-04
60	0,00747	-0,41530	0,00005	-0,00004	0,00602	-0,00598	43,66200	-2,19193	42,59057	2,5436E-04
65	0,00615	-0,41104	0,00008	-0,00006	0,00512	-0,00597	43,62368	-1,90357	42,56694	2,3862E-04
70	0,00506	-0,40754	0,00009	-0,00007	0,00417	-0,00597	43,59189	-1,60021	42,55400	2,2282E-04
75	0,00388	-0,40483	0,00010	-0,00009	0,00319	-0,00597	43,56687	-1,28477	42,55185	2,0748E-04
80	0,00278	-0,40292	0,00012	-0,00010	0,00219	-0,00596	43,54884	-0,95939	42,56052	1,9321E-04
85	0,00145	-0,40182	0,00013	-0,00011	0,00117	-0,00596	43,53790	-0,62702	42,57991	1,8073E-04
90	0,00021	-0,40156	0,00014	-0,00012	0,00014	-0,00596	43,53416	-0,28974	42,60990	1,7084E-04

Data sheet - Linear actor

THOMSON
Linear Motion. Optimized.™

Max Jac

12 and 24 Vdc - load up to 30 lb

» Ordering Key - see page 60
» Glossary - see page 61

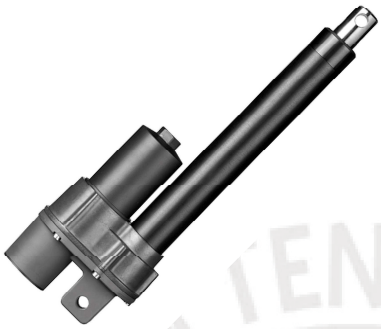

Standard Features and Benefits

- Designed for industrial applications
- Rugged aluminum housing with IP69K
- High efficiency
- Long life
- Hard coat anodizing for high corrosion resistance
- Virtually maintenance free
- Worm or ball screw models
- Non contact analog position feedback signal

General Specifications

Parameter	Max Jac
Screw type	worm or ball
Internally restrained	no
Manual override	no
Dynamic braking	no
Self locking worm screw models ball screw models	 yes no
End of stroke protection	no
Mid stroke protection	no
Motor protection	no
Motor connection	flying leads or cable with connector
Motor connector	AMP Superseal Series 1,5
Certificates	CE
Options	Encoder position feedback

Performance Specifications

Parameter		Max Jac
Maximum load, dynamic / static MX • • W (worm screw) MX • • B (ball screw)	[N]	 500 / 2000 800 / 100 - 350 [1]
Speed, at no load / at maximum load MX • • W (worm screw) MX • • B (ball screw)	[mm/s]	 33 / 19 60 / 30
Available input voltages	[VDC]	12, 24
Standard stroke lengths	[mm]	50,100,150 200, 250 [2], 300 [2]
Operating temperature limits	[°C]	-40 to +85
Full load duty cycle @ 25 °C	[%]	25
End play, maximum	[mm]	0,3
Restraining torque	[Nm]	2
Lead cross section	[mm²]	1
Standard cable lengths	[mm]	300, 1600
Protection class		IP66/IP69K
Salt spray resistance	[h]	500
Life	[cycles]	500000 [3]
Analog position feedback signal	[VDC]	0,5 - 4,5
Encoder position feedback option Supply voltage Pulses per mm, worm / ball screw Channels	[VDC]	 5 9,86 / 5,84 A, B

[1] The static force (i.e. the backdriving force) for a ball screw unit varies and is dependant on the number of cycles it have been running and at wich loads.

[2] Strokes possible for ball screw models only.

[3] For ball screw actuator with 100 mm stroke, average load of 500 N and changing load direction.

Duty Cycle vs. Load

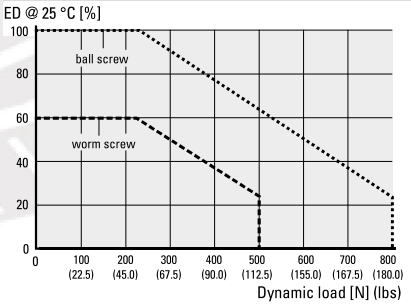

Max Jac

12 and 24 Vdc - load up to 30 lb

Dimensions	Projection
METRIC	

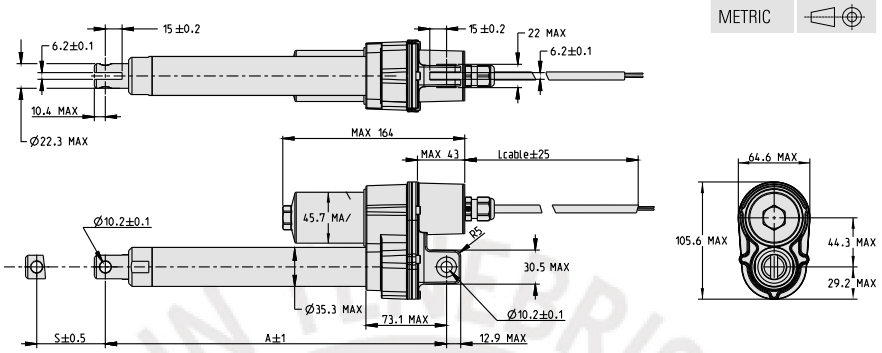

Stroke (S)	[mm (inch)]	50 (1.97)	100 (3.94)	150 (5.91)	200 (7.87)	250 (9.84) *	300 (11.81) *
Retracted length (A)	[mm (inch)]	206 (8.11)	256 (10.08)	306 (12.05)	356 (14.02)	406 (15.98)	456 (17.95)
Weight	[kg]	1,5	1,7	1,9	2,1	2,2	2,4

* Strokes possible for ball screw models only.

Performance Diagrams

Worm Screw Models (MX • • W)

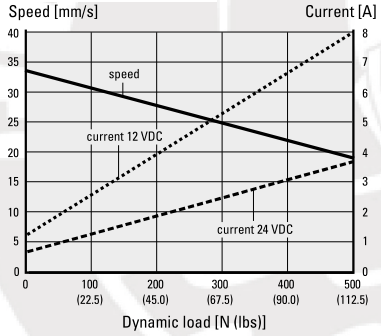

Ball Screw Models (MX • • B)